Global and Planetary Change 228 (2023) 104211

Contents lists available at ScienceDirect

Global and Planetary Change

journal homepage: www.elsevier.com/locate/gloplacha

Triassic-Jurassic vegetation response to carbon cycle perturbations and climate change

Remco Bos [a,*], Sofie Lindström [b], Han van Konijnenburg-van Cittert [a], Frederik Hilgen [a], Teuntje P. Hollaar [c,d], Hendrik Aalpoel [a], Carolien van der Weijst [a], Hamed Sanei [e], Arka Rudra [e], Appy Sluijs [a], Bas van de Schootbrugge [a]

[a] Department of Earth Sciences, Faculty of Geosciences, Utrecht University, Princetonlaan 8, 3584, CB, Utrecht, the Netherlands
[b] Department of Geosciences and Natural Resource Management, Copenhagen University, Øster Voldgade 10, DK-1350 Copenhagen K, Denmark
[c] WildFIRE Lab, Global Systems Institute, University of Exeter, Exeter, EX4 4PS, UK
[d] Camborne School of Mines, Department of Earth and Environmental Science, University of Exeter, Penryn Campus, Penryn TR10 9FE, UK
[e] Lithospheric Organic Carbon (LOC) Group, Department of Geoscience, Aarhus University, Høegh-Guldbergs gade 2, 8000C Aarhus, Denmark

ARTICLE INFO

Editor: Dr. Maoyan Zhu

Keywords:
End-Triassic Mass-Extinction
Early Jurassic
Terrestrial palynology
Vegetation disturbance
Central Atlantic Magmatic Province
Carbon cycle
Climate variability

ABSTRACT

Disturbances in terrestrial vegetation across the end-Triassic mass-extinction (ETME) and earliest Jurassic (~201.5–201.3 Ma) have previously been linked to carbon cycle perturbations induced by the Central Atlantic Magmatic Province. Large-scale volcanic degassing has been proposed to have affected the terrestrial realm through various mechanisms. However, the effects of long-term "super greenhouse" climate variability on vegetation dynamics following the mass-extinction remain poorly understood. Based on a 10-million-year long multi-proxy record of northern Germany (Schandelah-1, Germany, paleolatitude of ~41°N) spanning the late Rhaetian to the Sinemurian (~201.5–190.8 Ma), we aim to assess mechanistic links between carbon cycle perturbations, climate change, and vegetation dynamics.

Based on a high-resolution palynofloral record a two-phased extinction emerges, confirming extinction patterns seen in other studies. The first phase is associated with a decline in arborescent conifers, coinciding with a negative carbon isotope excursion and an influx of aquatic palynomorphs. Following this decline, we find a stepwise rise of ferns at the cost of trees during the latest Rhaetian, culminating with the extinction of tree taxa at the Triassic-Jurassic boundary. The rise in ferns is accompanied by an increase in reworked organic matter and charcoal, suggestive of erosion and wildfires. Furthermore, the Hettangian (201.3–199.3 Ma) vegetation in NW Europe shows evidence of long-term disturbance reflected by the periodic resurgence of fern taxa, similarly accompanied by increases in reworking and charcoal. This periodicity is linked to the 405-kyr eccentricity cycle indicating a biome that responded to astronomically induced variability in hydrology. A transition into an apparently more stable biome starts during the early Sinemurian, where palynofloral assemblages become dominated by bisaccate pollen taxa, mainly derived from conifers.

The ETME was clearly forced by the effects of volcanogenic emissions, such as SO_2, CO_2 and other pollutants, acting on both short (0.1–10 kyrs) and long timescales (10–100 kyrs). In contrast, charcoal and detrital input indicators show that the disturbances during the Hettangian were driven by periodic shifts in the regional hydrological regime. This was forced by the effects of orbital insolation variation and potentially exacerbated by increased atmospheric pCO_2. The cyclic progression of ecosystem disturbance was similar to that of the ETME and only recovered during the early Sinemurian. Atmospheric pCO_2 remained elevated after CAMP-activity had subsided due to a collapse of terrestrial biomass and carbonate producers. This inability to store carbon on long timescales could therefore have impeded global recovery.

* Corresponding author at: Princetonlaan 8a, 3584, CB, Utrecht, the Netherlands.
E-mail address: r.bos@uu.nl (R. Bos).

https://doi.org/10.1016/j.gloplacha.2023.104211
Received 24 February 2023; Received in revised form 31 July 2023; Accepted 31 July 2023
Available online 8 August 2023

1. Introduction

The emplacement of the Central Atlantic Magmatic Province (CAMP) that marked the initial break-up of Pangea, occurred synchronously with the end-Triassic mass extinction (ETME, ~201.3 Ma) and is generally held responsible for this major biotic crisis (Wignall, 2001; Bond et al., 2014; Lindström et al., 2019). Several distinct increases in pCO_2 across the TJ transition have been inferred from the stable carbon isotopic composition ($\delta^{13}C$) of soil carbonate nodules suggesting a doubling of Triassic values to nearly 5000 ppm during the earliest Jurassic (Schaller et al., 2011; Schaller et al., 2012). Stomatal density/size records, seem to confirm an earliest Jurassic rise in atmospheric pCO_2 from 1000 to 2000–3000 ppm (McElwain et al., 1999; Steinthorsdottir et al., 2011), resulting from the release of up to 8000 Gt of volcanogenic CO_2 (Beerling and Berner, 2002). The strong rise in atmospheric pCO_2 (Steinthorsdottir et al., 2011) is also believed to be the main trigger of major environmental upheaval with potential long-lasting consequences (Hesselbo et al., 2002; Ruhl and Kürschner, 2011).

Although the ecological devastation is well-constrained in faunal extinctions (Benton, 1990; Benton, 1995; Alroy, 2008), taxonomic losses in the plant-kingdom are more ambiguous and locally restricted with a selective impact, varying globally between 17 and 73%, based on spore and pollen taxa (McElwain and Punyasena, 2007; Mander et al., 2010; Lindström, 2016). Many detailed studies have focused on the link between CAMP-induced carbon cycle perturbations and the active destruction and/or extirpation of terrestrial vegetation during the ETME and lowermost Hettangian, mostly at northern hemisphere sites (McElwain et al., 1999; McElwain and Punyasena, 2007; van de Schootbrugge et al., 2009; Mander et al., 2010; Bonis and Kürschner, 2012; Li et al., 2016; Peng et al., 2018; Lindström et al., 2019; Li et al., 2020; Lindström, 2021; Lindström et al., 2021).

Curiously, only a single family, the peltaspermalean seed-ferns, went truly extinct (McElwain et al., 2007; McElwain et al., 2009), although evidence from Patagonia suggest some lineages of this family might have survived the Triassic-Jurassic transition (Elgorriaga et al., 2019). Most plant lineages show great resilience during this episode of severe environmental upheaval (van de Schootbrugge et al., 2009; Cascales-Miñana and Cleal, 2012). The two main pulses of increased extinction rates (Wignall and Atkinson, 2020; Lindström, 2021) coincide with negative excursions in the stable carbon isotopic composition ($\delta^{13}C$) of the global exogenic carbon pool, revealing that pulses in CAMP activity impacted terrestrial vegetation and marine biota. The first pulse mainly impacted arborescent conifers (Lindström, 2021) that were transiently replaced by pioneering spore-producing ferns, and fern allies (horsetails and mosses) flourishing in the vacated open landscapes (van de Schootbrugge et al., 2009; van Konijnenburg-van Cittert et al., 2020; van Konijnenburg-van Cittert et al., 2021; van Konijnenburg-van Cittert et al., 2022). The ETME culminated with the extinction of tree taxa at the Triassic-Jurassic boundary and resulted in major turnovers in dominant plant biomes (McGhee et al., 2013; Lindström, 2016) establishing Early Jurassic vegetation and a significant component of present-day flora (Rees et al., 2000). The exact timing of terrestrial recovery, however, remains unclear.

Although the ETME has been extensively studied, little information exists regarding the long-term impact of climate and carbon cycle variability induced by volcanism on the stability of terrestrial vegetation biomes during the Early Jurassic. The few available Early Jurassic records across the European continent revealed the presence of orbital pacing both in the exogenic carbon pool and vegetation assemblages. These are commonly linked through wildfire, erosional and monsoonal activity (Bonis et al., 2010; Storm et al., 2020; Hollaar et al., 2021). But to evaluate the ability of land plants to pass through severe bottleneck events such as the ETME and re-establish themselves, long-term records are required that allow to assess the role of climate change.

Here, we present a 10-million-year long palynological record obtained from shallow marine deposits from the Schandelah-1 core in the North German Basin spanning from the late Rhaetian to the late Sinemurian (~201.5 Ma to ~190.8 Ma). The high accumulation rates and continental proximity of the Schandelah-1 core (van de Schootbrugge et al., 2019) allows examination of the linkage between carbon cycle perturbations, climate change and vegetation preceding, during and following the ETME. We expanded the resolution of the bulk organic $\delta^{13}C$ record and combine this with organic matter characterisation for an assessment of shifts in regional carbon sourcing in relation to general carbon cycle dynamics. Furthermore, we assess climate-induced terrestrial ecosystem changes across the Triassic-Jurassic transition and into the Early Jurassic. We achieve this by evaluating palynofloral distribution and diversity patterns and subsequently comparing this record with contemporaneous sections across Europe to assess the geographic scale of recorded changes.

2. Background

2.1. Regional setting

The Late Triassic/Early Jurassic world was characterized by relatively high sea-levels, resulting in large epicontinental seas (Manspeizer, 1994; Martindale et al., 2015; Golonka et al., 2018). Northwest Europe was covered by an epicontinental seaway with isolated small cratonic landmasses. Depositional regimes varied between marginal fluvio-lacustrine and shallow marine settings (Fig. 1). The European Epicontinental Seaway (EES) was situated at mid-latitudes (30–50°N) during the transition from the Late Triassic to the Early Jurassic. The Central European Basin (CEB) was flanked by several emerging cratonic landmasses, such as the Bohemian, Rhenish and London-Brabant Massifs and the large continental area of the Fennoscandian Shield to the north. Marine connection to the high-latitude Arctic shelf area was established through the Viking corridor, while the Western Tethys shelf provided access to the Tethys Ocean to the south. The northernmost extent of the CAMP eruptions reached up to latitudes of 35°N across Iberia and possibly even southern France and Brittany (Caroff and Cotten, 2004). This puts many European sites in a proximal position to major volcanic activity, particularly given dominating south westerly winds at these latitudes.

The Schandelah-1 drill site is situated in the middle of the CEB in close proximity to the Rhenish Massif to the south (Fig. 1). Previous work documented pulses of reworked Ordovician, Silurian and Devonian palynomorphs in the uppermost Rhaetian suggesting exposure and weathering of cratonic landmasses such as the Bohemian Massif, Baltic Basin, and Fennoscandian Shield intensified during the latest Triassic (van de Schootbrugge et al., 2020). Results from other well-studied sites across this basin are included here for palynological reference allowing to present a broader window on vegetation development around the CEB. The Mingolsheim section of southern Germany (van de Schootbrugge et al., 2009; Lindström et al., 2017), Bonenberg section of northern Germany (Gravendyck et al., 2020) and Stenlille sections from Denmark (Lindström et al., 2012; Lindström et al., 2017) flank the CEB to the south and north, respectively. Palynological representation from the Eiberg Basin, south of the Bohemian Massif, is derived from the Kuhjoch Global Stratotype Section and Point (GSSP) site (Bonis et al., 2009). In addition, we utilize the well-studied St Audrie's Bay section from the UK for its high resolution palynostratigraphic reconstruction, which extends well into the Early Jurassic (Bonis et al., 2010). Placing the Schandelah records in the context of surrounding NW European sites will improve our understanding on vegetation gradients from all sides of the CEB.

2.2. Stratigraphic framework

The stratigraphic framework for the Triassic-Jurassic transition is based on several marine fossil groups including ammonites, bivalves, echinoderms, brachiopods, and conodonts. Particularly ammonites have

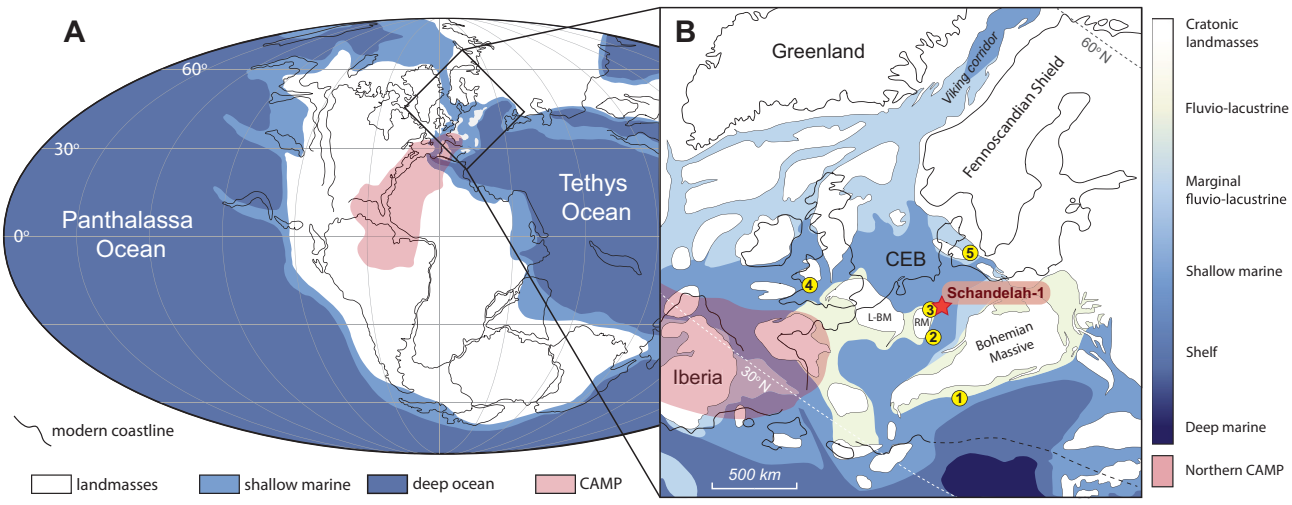

Fig. 1. Paleogeographic reconstruction of the end-Triassic. **A.** Global reconstruction of continental configuration and position of the Panthalassa and Tethys Oceans (modified after Martindale et al. (2015) and Golonka et al. (2018)). **B.** European Epicontinental Seaway with positions of previously studied palynological sections: 1. Kuhjoch (Austria, Bonis et al., 2009; von Hillebrandt et al., 2013), 2. Mingolsheim (Germany, van de Schootbrugge et al., 2009), 3. Bonenburg (Germany, Gravendyck et al., 2020), 4. St. Audrie's Bay (UK, Bonis et al., 2010; Bonis and Kürschner, 2012), 5. Stenlille (Denmark, Lindström et al., 2012). The red star indicates the position of the Schandelah-1 drill-core in northern Germany (this study). Modified after Blakey (2014), Lindström et al. (2015) and Schobben et al. (2019). (For interpretation of the references to colour in this figure legend, the reader is referred to the web version of this article.)

proven useful to link sites across the EES. The base of the Jurassic is synonymous with the first occurrence of the first ammonite *Psiloceras spelae tirolicum* (von Hillebrandt et al., 2007; von Hillebrandt and Krystyn, 2009; von Hillebrandt et al., 2013) based on the GSSP site at Kuhjoch. However, several sections of the Kuhjoch locality show faults and potential gaps in the sedimentary record. Although the first occurrence (FO) of *P. spelae* is considered to be synchronous across the Eiberg Basin, continental wide correlation seems problematic due to incomplete stratigraphic successions and biogeographical variability. Stratigraphic correlations have since been improved using $\delta^{13}C$ records, using two distinct negative carbon isotope excursions (CIEs), known as the Marshi ("precursor") and Spelae ("initial") CIEs, which reflect the volcanic injection of ^{13}C-depleted carbon (Hesselbo et al., 2002; Deenen et al., 2010; Ruhl et al., 2010b; Whiteside et al., 2010; Lindström et al., 2012; Corso et al., 2014). The Marshi CIE is considered the onset of the ETME, synonymous with the LO of the ammonoid *Choristoceras marshi* (von Hillebrandt et al., 2013).

High precision U-Pb dating suggest the oldest CAMP intrusions at 201.635 ± 0.029 Ma (Kakoulima intrusion, Guinea), 201.612 ± 0.046 Ma (Tarabuco sill, Bolivia) and 201.585 ± 0.034 Ma (Messejana dyke, Spain). Intrusions associated with the Marshi CIE date roughly to 201.564 ± 0.015 Ma (Newark Basin, USA) based on combining U-Pb dating with cyclostratigraphy and the LO of *C. marshi*, which reflects the onset of ETME Blackburn et al., 2013). Other U-Pb dated sills indicate ages of 201.525 ± 0.065 Ma (Solimões Basin, Davies et al., 2017) and 201.477 ± 0.062 (Amazon Basin, Heimdal et al., 2018), which span and possibly post-date the ETME, respectively (Heimdal et al., 2018). The youngest sill intrusions in the Amazon Basin reveal an approximate age of 201.364 ± 0.023 Ma and likely occur synchronously with the Spelae CIE (Heimdal et al., 2018) based on correlations of T-J boundary sections (Lindström et al., 2017). All U-Pb dates are reported for the same isotopic tracer and therefore require only the internal analytical uncertainties for comparison. Independently dated sections using ammonite biostratigraphy in Peru contain ash beds, of which radiometric ages place the TJB at 201.36 ± 0.17 Ma (Schaltegger et al., 2008; Schoene et al., 2010). The main pulses of extinction seem to coincide with the two negative CIEs based on mass rarity events in marine invertebrate and terrestrial palynology (Lindström et al., 2017; Wignall and Atkinson, 2020; Lindström, 2021).

From a palynological perspective, *co*-occurrence of the fern spore *Polypodiisporites polymicroforatus* and the enigmatic gymnosperm pollen taxon *Ricciisporites tuberculatus* provide excellent markers for stratigraphic correlation (Lindström et al., 2017). Particularly, the abundance of *P. polymicroforatus* culminates in a so-called "fern spike" (van de Schootbrugge et al., 2009) and can be traced across the northern German Basin (Lindström et al., 2017). The abundance of *R. tuberculatus* shows more spatial variability. The transition to the Early Jurassic (Hettangian) is marked by the pollen-taxon *Cerebropollenites thiergartii,* which occurs close the FO of the ammonite *P. spelae* (Kuerschner et al., 2007) in the Eiberg Basin in Austria. A number of last occurrences (LO) of Rhaetian marker species include the pollen-taxa *Lunatisporites rhaeticus*, *Ovalipollis ovalis*, *Ricciisporites tuberculatus*, *Rhaetipollis germanicus* and the last common occurrence (LCO) of the dinoflagellate species *Rhaetogonyaulax rhaetica* and thus have similar correlative potential (Bonis et al., 2010; Lindström et al., 2017; Gravendyck et al., 2020). Overall, terrestrial palynological assemblages seems to be indicative of phased, regional perturbations in vegetation composition occurring synchronously across the European continent. However, the biostratigraphy of the Hettangian and Sinemurian is largely based on ammonite biostratigraphy, while the terrestrial vegetation progression is poorly understood.

2.3. Lithology and biostratigraphy

The Schandelah-1 core was drilled near the German city of Braunschweig in 2008, yielding a 338 m succession of continuous strata ranging from Rhaetian to Toarcian age. Initial results were presented by van de Schootbrugge et al. (2019) with detailed descriptions of lithology, biostratigraphy, and carbon isotope stratigraphy. In summary (Fig. 2), the Rhaetian (338.0–318.6 m below surface (mbs)) can be subdivided into two formations based on lithology. The lower part belongs to the Arnstadt Formation (338.0–334.8 mbs) containing grey, brown, and green silt/claystone, reflecting a shallow marine environment based on the presence of the dinoflagellate cyst *Lunnomidinium scaniense*. A sharp transition to the medium-grained, cross-stratified sandstones of the overlying Exter Formation (334.8–318.6 mbs) marks the shift to a deltaic setting. This formation can be further subdivided into the Contorta Beds (334.8–332.0 mbs) containing clayey intervals, charcoal and plant remains and the Triletes Beds (332.0–318.6 mbs) mostly comprising fine to medium, grey sandstone. The Triletes Beds are

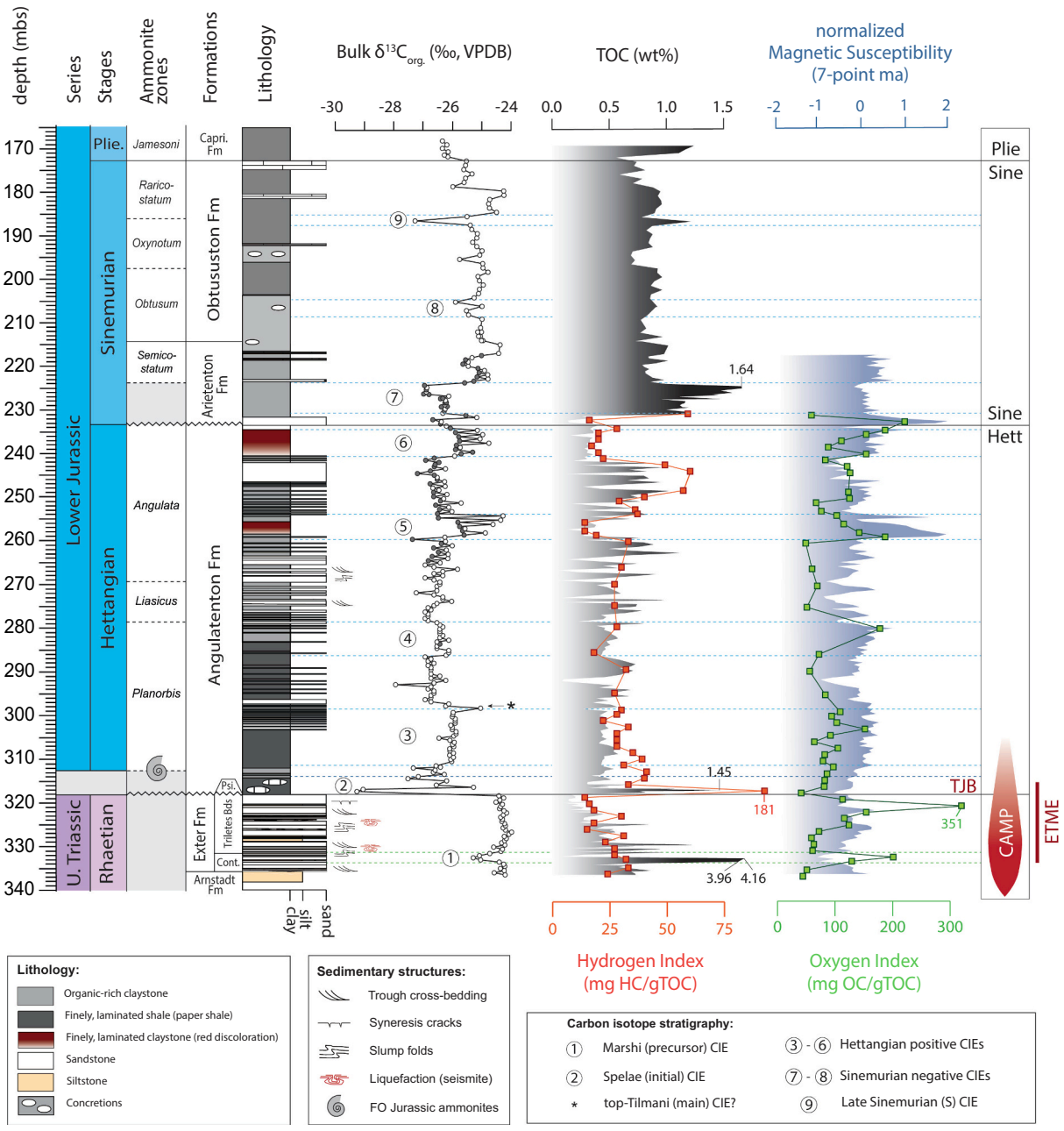

Fig. 2. Geochemical measurements of studied section from Schandelah-1 core. Lithostratigraphy and ammonite bio-zonation are derived from (van de Schootbrugge et al., 2019) and indicates a range of late Rhaetian to Sinemurian. Bulk organic carbon isotope record (VPDB = Vienna Peedee Belemnite) with numbers and dashed lines denoting several stages in the stratigraphy. Open data points represent the record presented by van de Schootbrugge et al. (2019) and solid grey data points represent newly generated data from this study. Total organic carbon concentrations are overlain by Hydrogen Index measurements. Normalized magnetic susceptibility record is presented by a 5-point moving average curve and overlain by Oxygen Index measurements. Position of CAMP activity and chronostratigraphic boundaries are depicted in right column.

dominated by muddy, bioturbated sandstone in the lower part and transitions to consistent laminated sandstone and interbedded shale facies in the upper part. In addition, the Triletes Beds contain liquefaction horizons that were interpreted as seismite deposits of *syn*-sedimentary nature. These liquefaction horizons can be traced across northern Europe, suggesting the late Rhaetian was plagued by repeated seismic activity (Lindström et al., 2015). Initial palynological examination revealed an abundance of *Polypodiisporites polymicroforatus* and *Ricciisporites tuberculatus* in the Triletes Beds, as well as the LCO of the dinoflagellate cyst taxon *Rhaetogonyaulax rhaetica*, confirming the late Rhaetian age and position of the ETME in the Schandelah-1 core (van de Schootbrugge et al., 2019). A sharp and irregular surface was recognized at the top of the Triletes Beds with a notable transition to distinctly different facies of the Psilonoten Sandstone (318.6–317.9 mbs).

The overlying Angulatenton Formation (Fig. 2; 318.6–233.3 mbs) of Hettangian age is mainly composed laminated dark-grey mudstone containing paper shales in the lower part (318.6–298.0 mbs). This interval contains sparse macrofossils, including a single occurrence of *Psiloceras* (*Neophyllites*?) at 312.2 mbs indicating the lower Jurassic Planorbis ammonite Zone (van de Schootbrugge et al., 2019). Additionally, an abrupt transition to a palynological assemblage typical of Early Jurassic vegetation is noted from 318.2 mbs including synchronous increases in the relative abundance of *Trachysporites fuscus* and *Pinuspollenites minimus* and the first common occurrence (FCO) of

Kraeuselisporites reissingerii. Therefore, the position of the Triassic-Jurassic boundary is placed between 319.5 and 318.2 mbs. Based on organic carbon isotope stratigraphy, which shows a notable negative excursion at 318.6 mbs, the T-J boundary is generally recognized at this position at the base of the Psilonoten Sandstone. The remainder to the Angulatenton Fm (298.0–233.3 mbs) is characterized by sandstone lenses (heteroliths), showing sometimes intense bioturbation, and cross-stratification (ripples, hummocks), alternating with organic-rich mudstone and shales. Ammonite biostratigraphy suggests that the Hettangian is mostly complete, with the Liassicus Zone represented by *Caloceras hercynum* and the upper Angulata Zone by several species of *Schlotheimia* sp. Two distinct intervals of finely laminated claystone are observed in the upper Angulatenton Fm (van de Schootbrugge et al., 2019).

The base of the Sinemurian consists of two hardground beds of calcareous sandstone (Arietes Sandstone, 233.3–230.2 mbs) and is associated with an unconformity at the Hettangian – Sinemurian boundary. The majority of the Sinemurian succession is characterized by well-laminated dark grey and black shales and organic-rich claystone and is further subdivided into the basal Ariententon Formation (233.3–214.0 mbs), and the Obtususton Formation (214.0–170.0 mbs). The presence of the ammonite *Arnioceras* gr. *semicostatum* indicates the Semicostatum ammonite Zone at the base of the Ariententon Fm. No ammonites belonging to either the Bucklandi or the Turneri Zones were found, suggesting a potential hiatus within the Ariententon Fm (van de Schootbrugge et al., 2019). In contrast, the Upper Sinemurian Obtusum ammonite Zone is well-presented by *Promicroceras* aff. *Precompressum*, *Promicroceras* gr. *planicosta*, and *Xipheroceras trimodum*. The uppermost ammonite zones of the upper Obtususton Fm (Oxynotum and Raricostatum Zones) are scarcely represented by ammonite groups of *Cleviceras* sp. and *Oxynoticeras* sp. The Sinemurian – Pliensbachian boundary is located at the base of the so-called "Doppelbank" based on the presence of the ammonite *Paltechioceras* at 172.0 mbs which may be indicative of the Denotatus Subzone (van de Schootbrugge et al., 2019).

3. Methodology

3.1. Palynological processing and quantification

A total of 186 samples were processed for palynology with an average resolution of 1 m for the Hettangian-Sinemurian (310–170 mbs) section and a higher resolution (0.3 m) for the upper Rhaetian-lowermost Hettangian section (338–310 mbs), expanding the records of van de Schootbrugge et al. (2019) and van Eldijk et al. (2018). All samples were oven-dried and approximately 5–7 g of material was crushed. A 132 samples were supplemented with a *Lycopodium* tablet for absolute quantification. Crushed material was subjected to a standard palynological protocol at Utrecht University and processed with 10% HCl solution for the removal of carbonates and dissolution of the *Lycopodium* tablet, and twice with 38% HF for the removal of siliciclastic elements. Every HF processing step was followed by a 30% HCl treatment to prevent the precipitation of calcium fluoride (CaF_2). Remaining material was sieved using a 10 μm nylon-mesh, homogenised and permanently mounted on glass slides using a combination of 5% Polyvinyl Alcohol (PVA) solution and glass glue. Palynological analysis of up to 300 palynomorphs was conducted where possible (95% of all samples) using light microscopy (40 × 10 magnification). Due to the overall low abundance of aquatic and other palynomorphs, terrestrial palynological records are presented as relative abundances (%) of the total palynomorph assemblage. In addition, the palynological slides were utilized to count the abundance of microcharcoal (10–250 μm) under a transmitted light microscope (40 × 10 magnification). The microcharcoal was identified based on the following characteristics: opaque/black in colour, sharp edges, often lath-like and preservation of the original anatomic features present (Scott, 2010). The abundance of charcoal is presented as the percentage of charcoal particles relative to all phytoclasts.

3.2. Organic carbon isotope record and organic matter characterisation

The $\delta^{13}C_{org}$ record of the Schandelah-1 core (van de Schootbrugge et al., 2019) covers the entire core (Rhaetian-Toarcian) representing a reference chemostratigraphic curve for the Lower Saxony Basin. A total of 253 samples covered the late Rhaetian to the late Sinemurian. Here we present an expanded $\delta^{13}C_{org}$ record with an additional 80 samples from the Hettangian, improving the resolution to about 0.5 m (Fig. 2). Powdered samples (~0.3 g) were treated twice using 10% HCl and rinsed with de-ionized water for the removal of carbonates, after which samples were homogenised and analysed for carbon content using a CNS-analyzer (NA 1500). The total organic carbon (TOC) content was calculated by multiplying the measured carbon content with ratio of the de-carbonated and original sample weights. Based on the resulting TOC values, homogenised and decarbonated residues, containing 30 μg of TOC, were analysed for $\delta^{13}C_{org}$ using a Fisons 1500 CNS Elemental Analyzer coupled to a Finnigan MAT Delta Plus mass spectrometer, bracketed by an in-house standard (Granite-Quartzite (GQ), accepted value = −26.68‰ VPDB). The GQ in-house standard value is determined by comparison with several internationally accepted standards. Accuracy and precision for the $\delta^{13}C_{org}$ measurements comprise 0.03‰ and 0.01‰, respectively. All results are reported relative to the Vienna Pee Dee Belemnite (VPDB). Both TOC and $\delta^{13}C_{org}$ measurements were performed at the department of Earth Sciences at Utrecht University.

In order to characterize organic matter, 53 powdered bulk samples (approximately 50 mg) covering the late Rhaetian and Hettangian were subjected to bulk pyrolysis geochemistry using a HAWK Pyrolysis and TOC instrument (Wildcat Technologies, USA) at Aarhus University based on the methods described in Rudra et al. (2021). This method follows the conventional Rock-Eval 6® method (Lafargue et al., 1998) during which the samples were subjected to the standard pyrolysis-oxidation cycle to produce the S_1 and S_2 peaks in a stepwise increase in temperature. The samples were pyrolyzed for 3 min at 300 °C (S_1 production) and is followed by a temperature increase to 650 °C with a ramp of 25 °C/min (S_2 production). The subsequent oxidation phase initiates with an isothermal stage for 1 min at 300 °C followed by a ramp of 25 °C/min up to 850 °C with a hold of 5 min. During pyrolysis the S_3 peak is produced from the carboxyl groups. The sum of the generative organic carbon (GOC, pyrolysis) and non-generative organic carbon (NGOC, oxidation) is used to calculated weighed percentages of TOC (wt %). The temperature of maximum rate of S_2 generation is considered to be T_{max} revealing the thermal maturity of the organic matter. The hydrogen index (HI) and oxygen index (OI) are calculated as follows; HI = (S_2/TOC)*100 (mg HC/g TOC) and OI = (S_3/TOC)*100 (mg CO_2/g TOC), respectively. The latter two indices reveal the ratio of hydrogen (H) and oxygen (O) relative to TOC, providing a glimpse into the state and potential source of the organic matter.

3.3. Magnetic susceptibility

A total of 290 samples were analysed for magnetic susceptibility (MS) with a resolution of 0.3–0.5 m. First, the weight of the bulk sample and of the 40 ml plastic vials containing the selected samples was determined. The weight of the plastic vials was determined to correct for potential contributing influence during the MS-measurements which was performed at room temperature using a AGICO MFK1-FA device. For the purpose of correcting for environmental and temperature-based influences, each sample was measured three times to assess the short-term reproducibility and variability, showing an average relative standard deviation of 0.151%. Duplicates were introduced to determine the long-term reproducibility during a single run, which showed no drift. The measurements were conducted using basic bulk magnetic susceptibility settings at a standard frequency of 976 Hz with a weak variable magnetic field of 200 A/m. Results were corrected for the total weight of

the sample. Due to the high sensitivity local measurement conditions, the MS record is presented in a normalized format to emphasize internal core variability. We present a 7-point moving average to assess the long-term trends in the record.

3.4. Statistical analyses

In order to extract palynofloral diversity dynamics and time series data, we utilize several techniques. To assess diversity, we study the richness (S; species and rarified richness ($n = 100$)), Shannon-Wiener index (H) and Pielou's Evenness. The Shannon-Wiener index (Shannon and Weaver, 1949) represents $H = -\Sigma p_i * \ln(p_i)$, where p_i is the proportion of species i (n_i/n), implying it is a function of relative abundances and the number of taxa. Pielou's Evenness (=eˆ(H/S)) normalizes to species richness. The computation of these indices was performed using the PAST 3 software (Hammer et al., 2001).

Spectral analysis was performed on both the magnetic susceptibility and $\delta^{13}C_{org}$ records using a 2π-multi-taper method (2π-MTM). Records were resampled to 0.1-m increments, detrended and filtered using the A-cycle software (Li et al., 2019). This analysis was performed in the depth scale and presented as such. Calculation of the significant frequencies were performed using a robust AR1 method (Mann and Lees, 1996) and presented by 90, 95, 99% confidence levels. Dominant frequencies were calculated as ratios to the stable long-eccentricity cycle (405 kyr) and extracted using Gaussian band-pass filters. Extracted dominant periods are superimposed over the original records for a comparative analysis.

4. Results

4.1. Organic carbon and $\delta^{13}C_{org}$

The Upper Triassic Rhaetian deposits show an overall steady $\delta^{13}C_{org}$ varying slightly between −24.1 to −24.6‰ (V-PDB) with one exception in the Contorta Beds at ~333 m revealing a negative CIE down to −25.8‰ (Fig. 2). This Contorta excursion has been identified as the Marshi (precursor) CIE (van de Schootbrugge et al., 2019) and is associated with the deposition of organic-rich siltstone with TOC levels up to 4.16%. The remaining TOC levels are typically below 0.5% with a gradual shift towards lower values (~0.2%) near the top of the Triletes Beds (325.5–318.8 mbs). The lowest TOC values correlate to the end-Triassic extinction (*P. polymicroforatus* abundance interval/fern spike). The transition into the Hettangian at 318.5 m is associated with a shift towards negative C-isotope values from −24.4 to −29.2‰ with a magnitude of 4.8‰. Values rapidly recover to −26.5‰ at 317 mbs. This excursion has been recognized as the Spelae (initial) CIE (Van de Schootbrugge et al., 2009). Part of the excursion may however be associated with a shift in organic matter composition associated with the sharp lithological transition from the sandstone of the Exter Fm to the finely laminated paper shale deposits of the lower Angulatenton Fm. The strong relation between minimum $\delta^{13}C_{org}$ values and a peak in TOC at the onset of the CIE corroborates this inference.

Average $\delta^{13}C_{org}$ values in the fluvial/deltaic sandstones of the Angulatenton Fm are −26.4‰. Shifts are typically associated with lithological boundaries. Four transient positive excursions of various magnitude represent laminated shale intervals (Fig. 2, excursion 3–6). Two intervals with strongly variable and generally higher $\delta^{13}C_{org}$ values have stable, low variability TOC content (<0.3%), while the lower $\delta^{13}C_{org}$ values show unstable, high variability TOC levels (0.1–1%). Most notable are the low, stable TOC levels associated with reddish clay intervals of the upper Hettangian (260–233.3 mbs), which show the most prominent positive $\delta^{13}C_{org}$ excursions with a magnitude of about 2‰. The lowermost interval of the Sinemurian (Arietes Sd, 233.3–230.2 mbs) indicates TOC levels similar to the red clay intervals of the upper Hettangian with one short-lived positive CIE to ~25.2‰. A subsequent transition to organic-rich claystone (230 mbs) shows a rapid increase in TOC from 0.2 to 1.2%, with $\delta^{13}C_{org}$ values remaining low at about −26.2‰ (Fig. 2, excursion 7). TOC values show a sharp decrease from ~1.5% to ~0.9% at 222.9 mbs and show minimal variation between 0.7 and 1% for the remainder of the Arietenton Fm. The $\delta^{13}C_{org}$ record stabilizes within the Obtususton Fm, fluctuating between −26 and −24.5‰. Two short-lived intervals can be recognized of slightly lighter values (Fig. 2, excursions 8 and 9). Excursion 9 occurs within the Oxynotum ammonite zone and is likely the late Sinemurian isotopic excursion (S-CIE) due to a co-occurrence with the dinoflagellate cyst *Liasidium variabile* (Riding et al., 2013). Most of the Obtususton Fm shows minimal variation in TOC values between 0.6 and 1% with a notable peak (1.2%) coinciding with the S-CIE.

4.2. Organic matter characterisation

The record variations in the Hydrogen Index (HI) and Oxygen Index (OI) (in mg HC/OC g^{-1} TOC) are indicative of the origin of the sedimentary organic matter (Wignall, 1994; Killops and Killops, 2013) (Fig. 2). Overall, the organic matter of the Schandelah-1 core typically consists of type-III kerogen (low HI and high OI) with one notable outlier at 318.5 mbs with a significantly higher HI value of 181 mg/g indicating mixed type-II/III kerogen associated with the Spelae CIE (Fig. S1). In line with expectations (Ruhl et al., 2010b; Killops and Killops, 2013), $\delta^{13}C_{org}$ values show a notable correlation ($R^2 = 0.42$) with the HI values (Fig. S2), although this is purely determined by the Rhaetian sand/siltstone samples, largely by a single data point (318.5 mbs, HI = 181 mg/g). An additional positive correlation is observed between HI and Hettangian TOC values ($R^2 = 0.430$). Although the majority of the Rhaetian and Hettangian samples show immature, type-III kerogen organic matter, we do observe stratigraphic variation that show similar patterns to TOC and bulk $\delta^{13}C_{org}$ values. OI positively correlates with magnetic susceptibility in the Hettangian records ($R^2 = 0.422$). The organic carbon records (HI and OI) and MS show the same periodic variability in the Angulatenton Fm and notable increases in the upper red clay intervals (258.5–254 mbs and 238–233 mbs). However, this relationship seems to be reversed in the Rhaetian, where we observe two short-lived peaks in OI values in interval with relatively low MS values. The first of these peaks in OI coincides with the Marshi CIE, while the second much larger peak occurs at the top of the Triletes Beds.

4.3. Palynology

4.3.1. Marker species biostratigraphy

The lowermost Arnstadt Fm interval can best be characterized by the pollen assemblage, which includes corystospermalean taeniate pollen *Lunatisporites rhaeticus*, alete bisaccates belonging to the morphogenus *Alisporites,* and *Ovalipollis ovalis*, a conifer pollen taxon. These taxa are consistently found in Rhaetian assemblages across Europe. This interval is here referred to as the *Lunatisporites-Alisporites* (LA) zone (Fig. 3). Minor occurrences of the enigmatic gymnosperm pollen *Ricciisporites tuberculatus* are also noted in this interval. Other notable appearances of spore taxa are *Polypodiisporites polymicroforatus* with an abundance up to 10%, and minor occurrences (<5%) of *Stereisporites* spp. (bryophytes), *Calamospora tener* (horsetails) and *Acanthotriletes varius*. Finally, we note minor occurrences of the lycopod spore *Zebrasporites laevigatus*, showing a consistent abundance (1–3%) throughout the entire lower succession of the Schandelah-1 core. The botanical affinities of all major recorded species are summarized in Table 1.

The base of the Contorta Beds also marks the initial occurrence of *Limbosporites lundbladiae* and *Rhaetipollis germanicus* which peaks at 334.0 mbs, although at low abundance (2%). Both these species gradually phase out towards the top of the Exter Fm. Additionally, these two taxa are commonly used to denote the *Rhaetipollis-Limbosporites* (RLi) Zone (Fig. 3) that is widely used for correlation across Europe (Lund, 1977; Kuerschner et al., 2007; Bonis et al., 2009; Lindström et al., 2017; Gravendyck et al., 2020). The overlying Triletes Beds is mainly dominated by *P. polymicroforatus* and other morphotypes of *Concavisporites-*

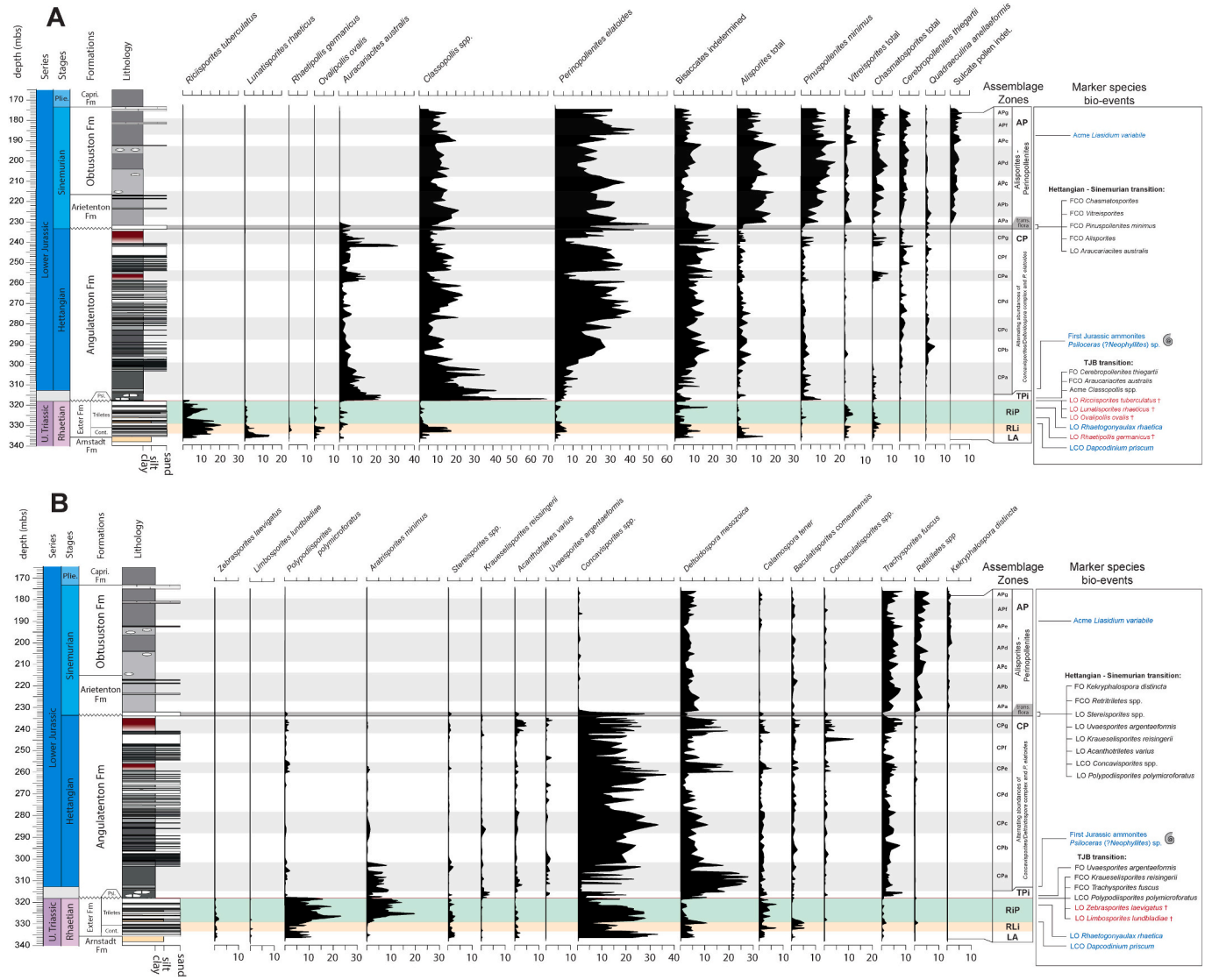

Fig. 3. Relative abundances of terrestrial palynology in the studied section of Schandelah-1 depicting significant occurrences of pollen-taxa (A) and spore-taxa (B). Palynofloral assemblage zones are derived by visual grouping of important marker species and bio-events: LA = *Lunatisporites-Alisporites*, RLi = *Rhaetipollis-Limbosporites*, RiP = *Ricciisporites-Polypodiisporites*, TPi = Trachysporites-Pinuspollenites, CP(a-g) = *Concavisporites-Perinopollenites*, trans. = transitional flora, AP(a-g) = *Alisporites-Perinopollenites*. Horizontal coloured bars indicate position of several palynofloral assemblage zones. Marker species bio-events denote the position of last occurrences (LO), last common occurrences (LCO), first occurrences (FO), first common occurrences (FCO) and acmes. Red lettering indicates main victims of Late Triassic crisis. Blue lettering indicates bio-events related to aquatic/marine species. (For interpretation of the references to colour in this figure legend, the reader is referred to the web version of this article.)

Deltoidospora, indicating the so-called "fern spike interval" (van de Schootbrugge et al., 2009). In addition, we note sporadic occurrences of *Limbosporites lundbladiae* in the *Ricciisporites-Polypodiisporites* (RiP) zone (Fig. 3) of the Triletes Beds. Other palynostratigraphic studies have also noted high abundances of *P. polymicroforatus* in this interval (Lindström, 2016; Lindström et al., 2017) and can be used to stratigraphically correlate the Late Triassic crisis among records across NW Europe.

The top of the Triletes Beds is capped by a sharp, irregular surface which transitions into the Psilonoten Sandstone (318.6–317.9 mbs) (van de Schootbrugge et al., 2019). In the upper meter (319.5–318.6 mbs) of the Exter Fm, marking the transition into the Jurassic, we record the disappearance of *Lunatisporites rhaeticus*, *Ovalipollis ovalis* and *Ricciisporites tuberculatus*, associated with the ETME. Another notable last occurrence includes the lycopod *Zebrasporites laevigatus* and the last common occurrence of *P. polymicroforatus* at 318.6 mbs. The exception is *Rhaetipollis germanicus* which disappears from our record within the Triletes Beds at 328.5 mbs. Near the base of the Angulatenton Fm (318.2 mbs), the first occurrence of *Cerebropollenites thiergartii* marks the base of the Jurassic. The first ammonites in the Schandelah-1 core occur at a depth of 312.1 mbs, well above the proposed base of the Hettangian. However, we observe an abrupt change to a clearly Early Jurassic palynofloral assemblage at 318.2, which includes the first common occurrence (FCO) of *Krauselisporites reissingerii* and first occurrence (FO) of *Uvaesporites argentaeformis*. In addition, at this level the FCO of *Trachysporites fuscus* and *Pinuspollenites minimus* indicates the position of the Triassic-Jurassic boundary between 318.6 and 318.2 mbs. This interval is noted as the *Trachysporites-Pinuspollenites* (TPi) zone (Fig. 3).

Based on ammonite biostratigraphy, the Hettangian-Sinemurian marks a sharp lithological transition from the shales and sands of the Angulatenton Fm to light grey, organic-rich claystone of the overlying Arietenton Fm (233.3 mbs) (van de Schootbrugge et al., 2019). The Sinemurian of Schandelah encompasses around 63 m of sediment containing 5 to 10% of aquatic palynomorphs throughout the Sinemurian (Fig. 4). This suggests a deepening of the basin consistent with the shift

Table 1
Botanical and ecological affinities of significant spore and pollen taxa. Affinities are derived from Mander (2011) and Lindström (2016).

Palynofloral taxon	Botanical affinity				Ecological affinity	
	Class	Order	Family	Reference	Parent group	Habitat
Spore taxa						
Concavisporites jurensis	Pteridopsida/ Filicopsida	Filicales	Dipteridaceae/Matonicaeae	van Konijnenburg-van Cittert (1993); Guignard et al. (2009)	ground/ tree ferns	understory/ ground cover
Deltoidospora mesozoica	Pteridopsida/ Filicopsida	Filicales	Cyanthaceae/Dicksoniaceae/ Dipteridaceae/ Matonicaeae	van Konijnenburg-van Cittert (1993) ; Balme (1995); Guignard et al. (2009)	ground/tree ferns	understory/ground cover
Baculatisporites comaumensis	Pteridopsida/ Filicopsida	Filicales	Osmundaceae	van Konijnenburg-van Cittert (2000)	ground/tree ferns	understory/ground cover
Conbaculatisporites spp.	Pteridopsida/ Filicopsida	Filicales	Dipteridaceae	Pedersen and Lund (1980)	ground/tree ferns	understory/ground cover
Zebrasporites leavigatus	Pteridopsida/ Filicopsida	Filicales	nd		ground/tree ferns	understory/ground cover
Polypodiisporites polymicroforatus	Pteridopsida/ Filicopsida	Schizaeales	Schizaeaceae	van de Schootbrugge et al. (2009)	ground/tree ferns	understory/ground cover
Trachysporites fuscus	Pteridopsida/ Filicopsida	nd	nd	Bonis et al. (2010)	ground/tree ferns	understory/ground cover
Acanthotriletes varius	Pteridopsida/ Filicopsida	nd	nd		ground/tree ferns	understory/ground cover
Retritriletes spp.*	Lycopodiopsida	Lycopodiales	Lycopodiaceae	Bonis and Kürschner (2012)	lycopods/ clubmosses	ground cover
Kraeuselisporites reissingerii	Lycopodiopsida	Selaginellales	Selaginaceae		lycopods/ clubmosses	ground cover
Uvaesporites argentaeformis	Lycopodiopsida	Selaginellales	Selaginaceae	Balme (1995); Looy et al. (2005)	lycopods/ clubmosses	ground cover
Densosporites sp.	Lycopodiopsida	Selaginellales	nd		lycopods/ clubmosses	ground cover
Limbosporites lundbladiae	Lycopodiopsida	Selaginellales	nd	Balme (1995)	lycopods/ clubmosses	ground cover
Aratrisporites minimus	Lycopodiopsida	Isoetales	nd		lycopods/ clubmosses	ground cover
Calamospora tener	Equisetopsida	Equisetales	Equisetaceae	Kelber and Konijnenburg-van Cittert (1998)	horsetails	ground cover
Stereisporites spp.	Sphagnopsida	Sphagnidae	Sphagnaceae	Askin (1990)	mosses	ground cover
Kekryphalospora distincta	nd	nd	nd		nd	nd
Pollen taxa						
Cerebropollenites thiergartii	Coniferopsida	Coniferales	Taxodiaceae	van Konijnenburg-Van Cittert and van der Burgh (1989)	conifers	canopy/ shrubs
Perinopollenites elatoides	Coniferopsida	Coniferales	Taxodiaceae	van Konijnenburg-Van Cittert and van der Burgh (1989)	conifers	canopy/shrubs
Araucariacites australis	Coniferopsida	Coniferales	Araucariaceae	Balme (1995)	conifers	canopy/shrubs

(*continued on next page*)

Table 1 (*continued*)

Palynofloral taxon	Botanical affinity				Ecological affinity	
Classopollis spp.	Coniferopsida	Coniferales	Cheirolepidiaceae	Harris (1979); Balme (1995)	conifers	canopy/shrubs
Quadraeculina anellaeformis	Coniferopsida	Coniferales	Podocarpaceae	Bonis et al. (2010)	conifers	canopy/shrubs
Pinuspollenites minimus	Coniferopsida/ Pinopsida	Pinales	Pineceae	Traverse (2007); Leslie (2008)	conifers	canopy/shrubs
Alisporites spp.	Coniferopsida/ Pteridospermopsida	Coniferales/ Corystospermales	Corystospermaceae	Osborn et al. (1993); Balme (1995); Traverse (2007)	seed ferns	shrubs
Lunatisporites rhaeticus	Coniferopsida/ Pteridospermopsida	Coniferales/ Corystospermales	Corystospermaceae	Balme (1995); Traverse (2007)	seed ferns	shrubs
Vitreisporites spp.	Pteridospermopsida	Caytoniales	nd	Batten and Dutta (1997)	seed ferns	shrubs
Chasmatosporites spp.	Cycadopsida/ Ginkgopsida	Cycadales/ Ginkgoales	nd		cycads/ginkgos	canopy
Rhaetipollis germanicus	nd	nd	nd		nd	nd
Ricciisporites tuberculatus	nd	nd	nd		nd	nd
Ovalipollis ovalis	nd	nd	nd		nd	nd

nd = not determined

* *Retriletes* spp. has been linked to belong to Marchantiales (liverworts)

in lithology. From a local perspective, this transition marks the last occurrences of the spore-taxa *Stereisporites* spp., *Uvaesporites argentaeformis*, *Kraeuselisporites reissingerii*, *Acanthotriletes varius* and *Polypodiisporites polymicroforatus*, as well as a last common occurrence of *Concavisporites* spp. The only notable local LO in pollen taxa is that of *Araucariacites australis*. The only significant first occurrence at the base of the Sinemurian is the spore taxon *Kekryphalospora distincta*, albeit in low abundance (<3%). This transition is marked as a transitional flora. Terrestrial palynological records show minimal variation and no clear events within the Sinemurian of the Schandelah-1 core. However, we do observe a spike in the occurrence of the dinoflagellate cyst *Liasidium variabile* (13% of the total palynological assemblage) at 183.30 mbs. Previous examinations of several other European records have noted this event to be synchronous across the EES and closely tied to the S-CIE in the Oxynotum ammonite zone (Riding et al., 2013).

4.3.2. Major palynofloral trends

The Rhaetian succession of the Schandelah-1 core (338–318.6 mbs) is dominated by terrestrial palynomorphs constituting between 93 and 100% of the total palynological assemblage (Fig. 4). The only exception is the Contorta Beds at the base of the Exter Fm (334.8–332.0 mbs). Here we observe a sharp and short-lived influx of aquatic palynomorphs (up to 28%) dominated by the dinoflagellate cyst taxa *Rhaetogonyaulax rhaetica* and *Dapcodinium priscum* (Plate I).

The major palynofloral trends are clearly reflected in the spore-pollen (S/P) ratio (Fig. 4) which is defined as the total spores over the sum of total pollen and spores (Σspores/(Σpollen+Σspores) reflecting the abundance of spores relative to pollen. The S/P record can be subdivided into three distinct intervals. (1) The upper Rhaetian assemblage (Exter Fm) shows a shift to extremely high dominance of spore-taxa (S/P ratio > 0.8), closely associated with the RiP assemblage zone. This interval denotes the position of the "crisis interval" which is associated with a diminishing presence and the disappearance of several major pollen-taxa. (2) The base of the Hettangian assemblages (Angulatenton Fm) at 318.5 mbs, is characterized by a sharp decrease in spore abundance (S/P ratio < 0.1). This rapid transition is associated with an unconformity. Overall, the Hettangian assemblages are characterized by lower spore abundances (average S/P ratio = 0.3) with periodic increases in spore dominance (S/P ratio = 0.6). These periodic increases correlate well with several subzones of the CP assemblage. (3) Lastly, the transition into Sinemurian assemblages at the base of the Ariententon Fm (233.3 mbs) shows another rapid decrease in spore abundance (S/P ratio = 0.2). We observe a brief increase in spore abundance (S/P ratio = 0.5) within the Arietes Sandstone (233.3–230.2 mbs) which is associated with a transitional flora. However, the majority of the Sinemurian assemblage (Ariententon Fm and Obtususton Fm) show minor influence of spore-taxa (average S/P ratio = 0.2) with little variation. Interestingly, the relative abundance of microcharcoal correlates well with the S/P ratio. A sharp increase in microcharcoal (~10% of total phytoclasts) can be observed near the bottom of the RiP assemblage zone (Triletes Beds), mirroring the dominance trend of spore-taxa. Similar increases in microcharcoal are present within the Angulatenton Fm and coincide with increases in S/P ratio. A notable exception in the lower Angulatenton Fm (CPa subzone). The highest observed microcharcoal abundance in the Angulatenton Fm (9.3%) is situated at 293.9 mbs. Transition to Sinemurian strata show a notable drop in the average abundance of microcharcoal (average = 2%). However, a single sample indicates microcharcoal abundance of ~8% in the lower Arietes Sandstone. This single spike corresponds with an increase in S/P ratio.

The major contributors to the palynofloral assemblages of the Rhaetian to Sinemurian from Schandelah-1 have been summarized in Plate II. The entire Rhaetian succession can be subdivided into four intervals characterized by a distinct palynofloral composition. (1) The Arnstadt Fm (338–334.6 mbs) is dominated by spore-producing taxa (up to 70%), notably, pteridopsid fern spores (*Concavisporites* spp. and *Deltoidospora mesozoica*) (up to 34%), suggesting a fern and fern-tree

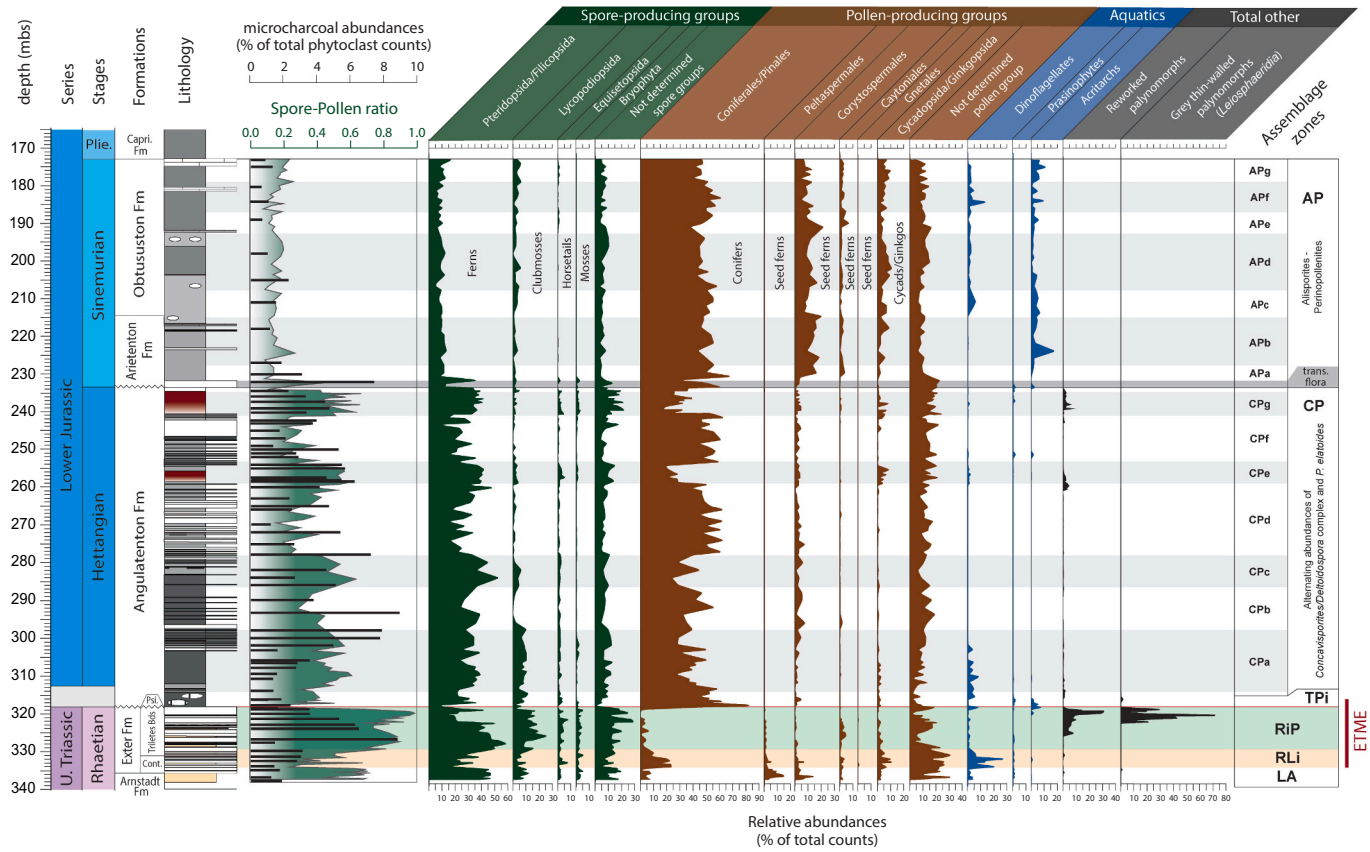

Fig. 4. Major vegetation patterns as inferred by their botanical affinities. Spore-pollen (S/P) ratio is defined as total spores over the sum of total pollen and spores (Σspores/(Σpollen+Σspores)) for each sample and is given in shaded green area. Relative microcharcoal abundances based on palynological slide material with black bars indicate position and magnitude of individual counts. All major spore/pollen producing groups are given in relative abundances (percentage of total assemblage). Major spore-producing groups are depicted in green. Major pollen-producing groups are depicted in brown. Additional relative abundances of aquatic groups and other palynomorphs are given in blue and black, respectively. (For interpretation of the references to colour in this figure legend, the reader is referred to the web version of this article.)

dominated landscape (Fig. 3-4). (2) The overlying Contorta Beds mark a shift to a pollen-dominated assemblage with high abundances of the cheirolepid conifers (*Classopollis* sp., 18%) and *R. tuberculatus* (21%), and the influx of dinoflagellate cysts (*Rhaetogonyaulax rhaetica* and *Dapcodinium priscum*). Abundances of taxodiaceous conifers (*Perinopollenites elatoides*), the pollen-taxa of *O. ovalis* and various types of bisaccate pollen, indicate a rich upper canopy tree vegetation. Nearly all spore-producing taxa show diminishing trends in the Contorta Beds except for horsetails (*Calamospora tener)* and osmundaceous ferns (*Baculatisporites comaumensis),* which experience minor and short-lived peaks. (3) At the base of the Triletes Beds (332.0 mbs), the entire assemblage shifts abruptly to a spore-dominated assemblage mainly represented by pteridopsid ferns (*P. polymicroforatus*, *Concavisporites* spp. and *D. mesozoica*) (up to 90%) and a group of isoetalean lycopods (*Aratrisporites minimus*) characteristic of humid, swamp-like conditions. This interpretation is further substantiated by the synchronous increase in horsetails (*C. tener*) and mosses (*Stereisporites* sp.) which require humid conditions for spore dispersal and reproduction. The only persistent pollen taxon *R. tuberculatus* shows a small peak at 324.1 mbs. (4) Finally, the top 3.5 m of the Exter Fm shows a dramatic increase in palynomorphs previously identified as Paleozoic acritarchs (van de Schootbrugge et al., 2020), peaking at 322.0 mbs (9.9%), attributed a major reworking spike due to catastrophic soil erosion. Additionally, a sharp increase of an unidentified grey-stained thin-walled sphaerical palynomorphs (Plate II), technically *Leiosphaeridia*, peaks at 320.8 mbs (71%) is closely tied to the reworking signal.

Similar to the underlying Rhaetian deposits, the Hettangian record shows an assemblage dominant in terrestrial palynomorphs with a near absence of aquatics. However, the lower part of the Hettangian (318.6–298.0 mbs), does show increased influence of aquatic dinoflagellate cysts varying up to 4%. The lowermost succession of the Hettangian (318.6–314.0) is characterized by a sharp shift towards a pollen-dominated assemblage comprised mostly of the conifers (*Classopollis torosus* and *Araucariacites australis*). Notable, are the pollen-taxa of *Classopollis* spp. which exhibits an acme of 70% at the base of the Hettangian (318.2 mbs). This pollen-dominance gradually tapers out towards the top of this interval, being transiently replaced by pteridopsid ferns (*D. mesozoica*, morphotypes of *Concavisporites* spp. complex and *Aratrisporites minimus*). The remainder of the Hettangian (314–233.3 mbs) shows four intervals of dominance in fern and fern allies (mainly *Deltoidospora mesozoica/Concavisporites* spp.) (Fig. 3-4; CPa,c,e and g subzones), alternating with three intervals of dominance in conifers (mainly *P. elatoides/Classopollis* sp.; CPb,d and f subzones). This alternation is regularly spaced through the Angulatenton Fm (Fig. 4; CPa-g subzones). Other taxa associated with the Hettangian mainly include vegetation that produces bisaccate-pollen which comprises roughly 20% of the total abundance which include seed ferns (*Alisporites* sp. and *Vitreisporites* sp.) and pinaceous conifers (*P. minimus*). Interestingly, bisaccate-producing vegetation does not show any clear cyclic pattern. Other plants that are consistently present during the Hettangian include cycads/ginkgos (*Chasmatosporites* sp.), taxodiaceous conifers (*Cerebropollenites thiergartii*) and podocarpaceous conifers (*Quadraeculina anellaeformis*). The remaining spore-bearing taxa of the Hettangian only show minor occurrences (<5%) throughout the Angulatenton Fm. These include mosses (*Stereisporites* spp.), horsetails (*Calamospora tener*), lycopods/clubmosses (*Kraeuselisporites reissingerii*, *Uvaesporites*

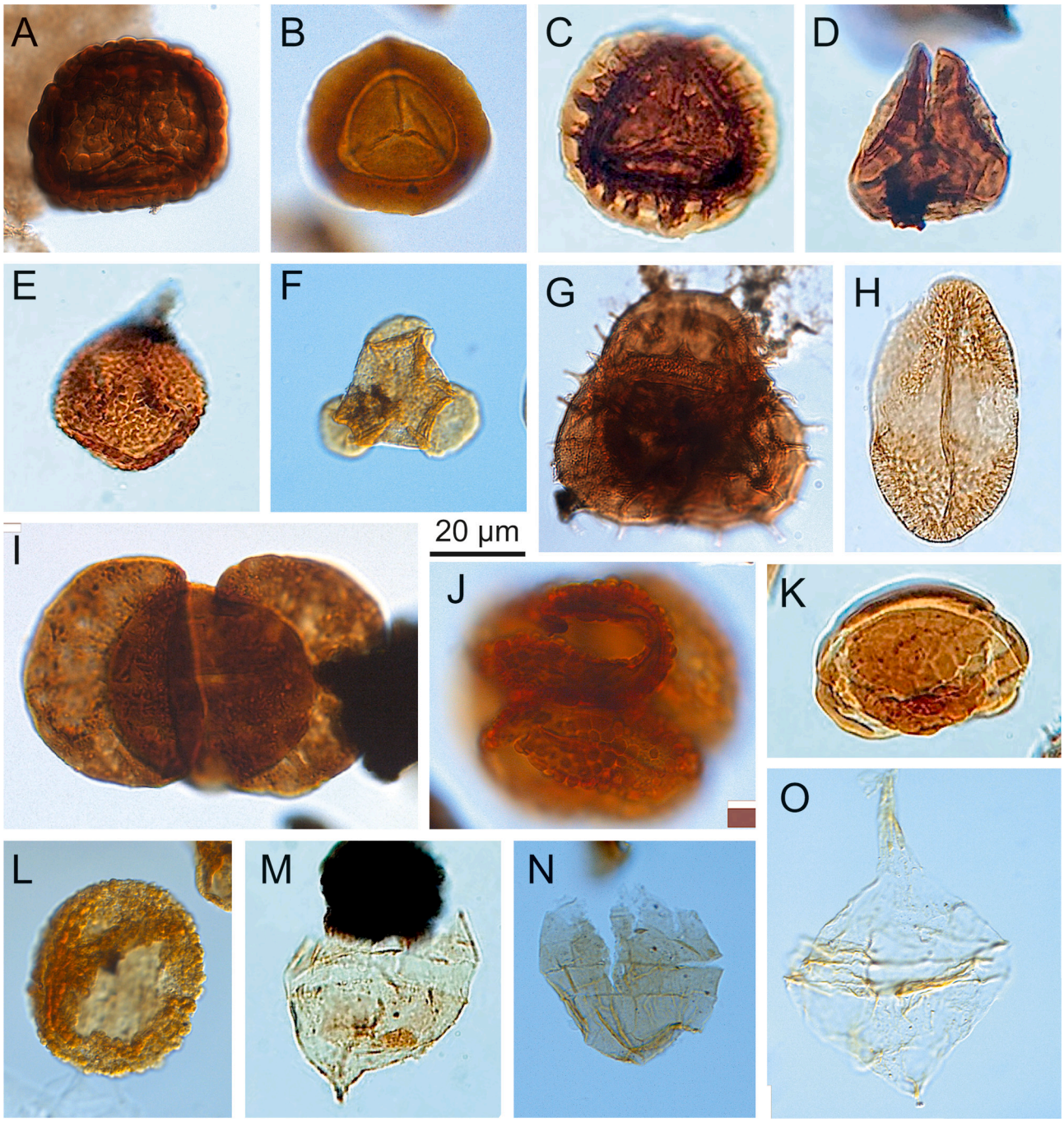

Plate I. Assemblage impression of palynofloral and algal marker species. A. *Uvaesporites argentaeformis* (317.10 mbs), B. *Densosporites fissus* (333.00 mbs), C. *Limbosporites lundbladiae* (328.50 mbs), D. *Zebrasporites* sp. (328.50 mbs), E. *Polypodiisporites polymicroforatus* (328.50 mbs), F. *Kekryphalospora distincta* (175.90 mbs), G. *Kraeuselisporites reissingerii* tetrad (317.10 mbs), H. *Ovalipollis ovalis* (333.20 mbs), I. *Lunatisporites rhaetica* (319.66 mbs), J. *Ricciisporites tuberculatus* tetrad (333.00 mbs), K. *Rhaetipollis germanicus* (332.50 mbs), L. *Cerebropollenites thiergartii* (216.00 mbs), M. *Rhaetogonyaulax rhaetica* (332.50 mbs), N. *Dapcodinium priscum* (332.50 mbs), O. *Liasidium variabile* (180.40 mbs).

argentaeformis and *Retitriletes* spp.), and ground ferns (*Acanthotriletes varius*, *Baculatisporites comaumensis* and *Conbaculatisporites* spp.). A notable exception is the occurrence of the pteridopsid fern of *Trachysporites fuscus* which shows abundances varying between 3 and 10%. Additionally, the part of the Angulatenton Fm marks the last common occurrence (LCO) of the lycopod *Aratrisporites minimus*, beyond which this species only occurs sporadically. The same can be said for most other spore-bearing taxa, having only minor occurrences (<5%) and mostly increasing their relative abundance during intervals of high pteridopsid ferns (*D. mesozoica/Concavisporites* spp.) abundance, exhibiting a cyclic nature. This cyclic behaviour is similarly noted for all pollen taxa following intervals of high conifer (*P. elatoides/Classopollis* sp.) abundance. Finally, the upper half of the Angulatenton Fm shows distinct the red clay-mudstone intervals during which cycads/ginkgos (*Chasmatosporites* sp.), and some conifers (*Araucariacites australis*) show high abundances.

The transition to the Sinemurian is characterized by a shift towards a pollen-dominated assemblage consisting mostly of bisaccate-producing vegetation (*Pinuspollenites minimus*, *Alisporites* spp. and *Vitreisporites* spp.) (Fig. 3, AP zone). This dominance of wind-dispersed pollen

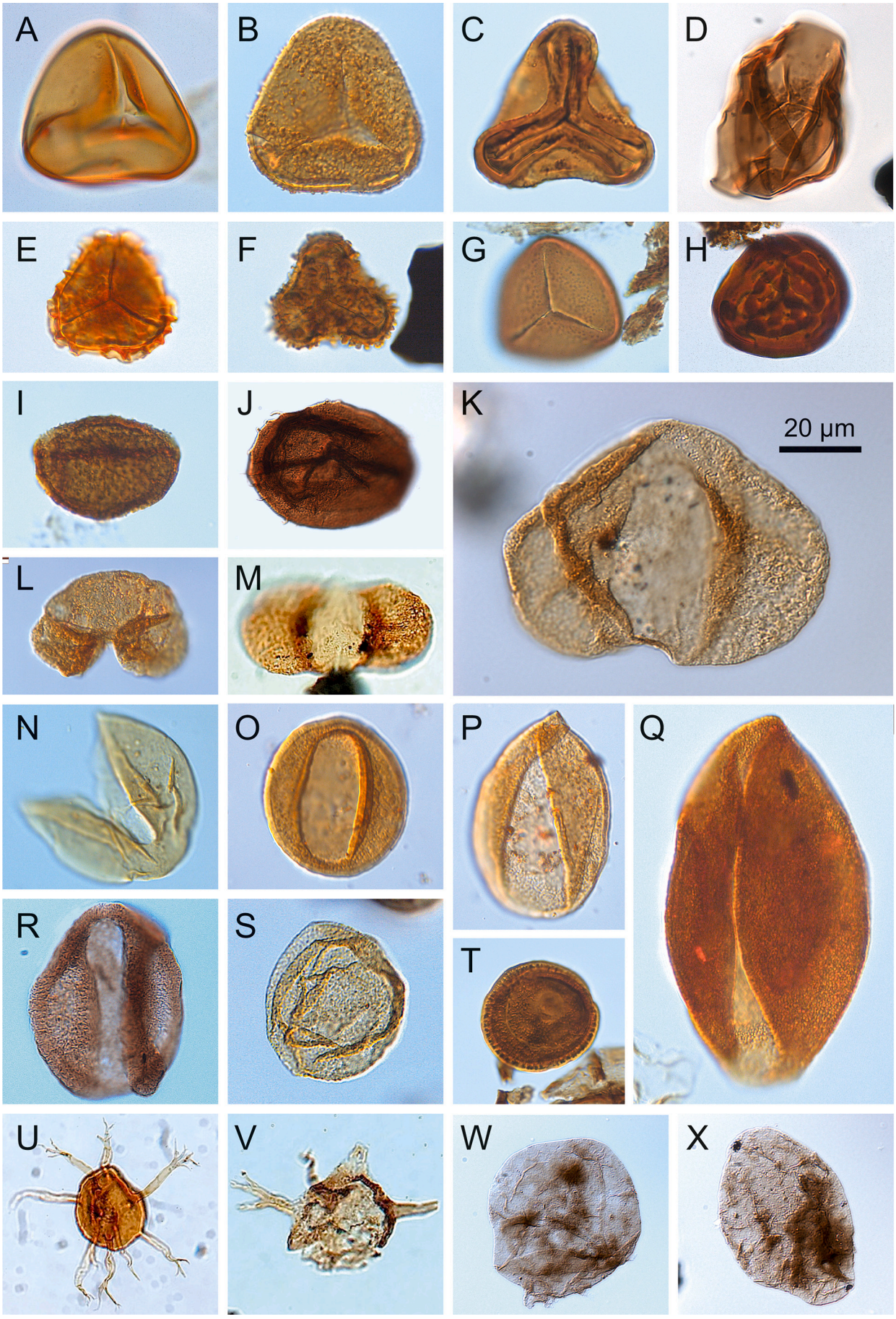

(caption on next page)

Plate II. Assemblage impression of significant palynofloral species. A. *Deltoidospora mesozoica* (332.50 mbs), B. *Trachysporites fuscus* (316.40 mbs), C. *Concavisporites jurensis* (245.00 mbs), D. *Calamospora tener* (325.00 mbs), E. *Retitriletes* sp. (233.90 mbs), F. *Acanthotriletes varius* (237.00 mbs), G. *Conbaculatisporites* sp. (332.50 mbs). H. *Stereisporites aulosenensis* (329.90 mbs), I. *Aratrisporites minimus* (316.40 mbs), J. *Aratrisporites palettae* (336.80 mbs), K. *Alisporites robustus* (304.00 mbs), L. *Pinuspollenites minimus* (316.40 mbs), M. *Vitreisporites bjuvensis* (328.50 mbs), N. *Perinopollenites elatoides* (175.90 mbs), O. *Chasmatosporites hians* (172.00 mbs), P. *Chasmatosporites elegans* (172.00 mbs), Q. *Chasmatosporites major* (235.20 mbs), R. *Quadraeculina anellaeformis* (333.50 mbs), S. *Araucariacites australis* (316.20 mbs), T. *Classopollis torosus* (249.00 mbs), U-V. Paleozoic acritarchs (reworked) (319.80 mbs), W-X. Grey-stained thin-walled sphaerical palynomorphs (*Leiosphaeridia*) (320.80 mbs).

similarly suggests a selective preservation consistent with relative sea level rise and a further distance to the coastline (Neves effect, Chaloner, 1958). Other notable increases include cycads/ginkgos (*Chasmatosporites* sp.). The taxodiaceous and pinaceous conifers (*Perinopollenites elatoides* and *Classopollis* sp.), dominant in Hettangian assemblages, show similar abundances in the Sinemurian, varying between 30 and 40% and 10–20%, respectively. Closer inspection reveals several alternating intervals marked by either a dominance of the mire-conifer *P. elatoides* or increased abundance of several bisaccate pollen taxa (*Alisporites* sp., *Pinuspollenites minimus* and *Vitreisporites* sp.) and several spore taxa (*Deltoidospora mesozoica*, *Baculatisporites comaumensis*, *Conbaculatisporites* spp., *Trachysporites fuscus*, *Retitriletes* spp., *Kekryphalospora distincta*). A total of seven subzones can be defined (APa – g subzones) with four intervals of increased *P. elatoides* (APa,c,e and g subzones) abundance and three intervals of increased bisaccate pollen and spore abundance (APb,d and f subzones). The minor presence (<3%) of podocarpaceous conifers (*Quadraeculina anellaeformis*) rounds off the significant composition of pollen taxa in the Sinemurian. The major components of the spore-bearing taxa include pteridopsid ferns (*D. mesozoica* and *T. fuscus*) and the first common occurrence of the lycopod *Retitriletes* spp. Other minor occurrences include *Baculatisporites comaumensis*, *Conbaculatisporites* spp., *Calamospora tener* and sporadic occurrences of *Concavisporites* spp.

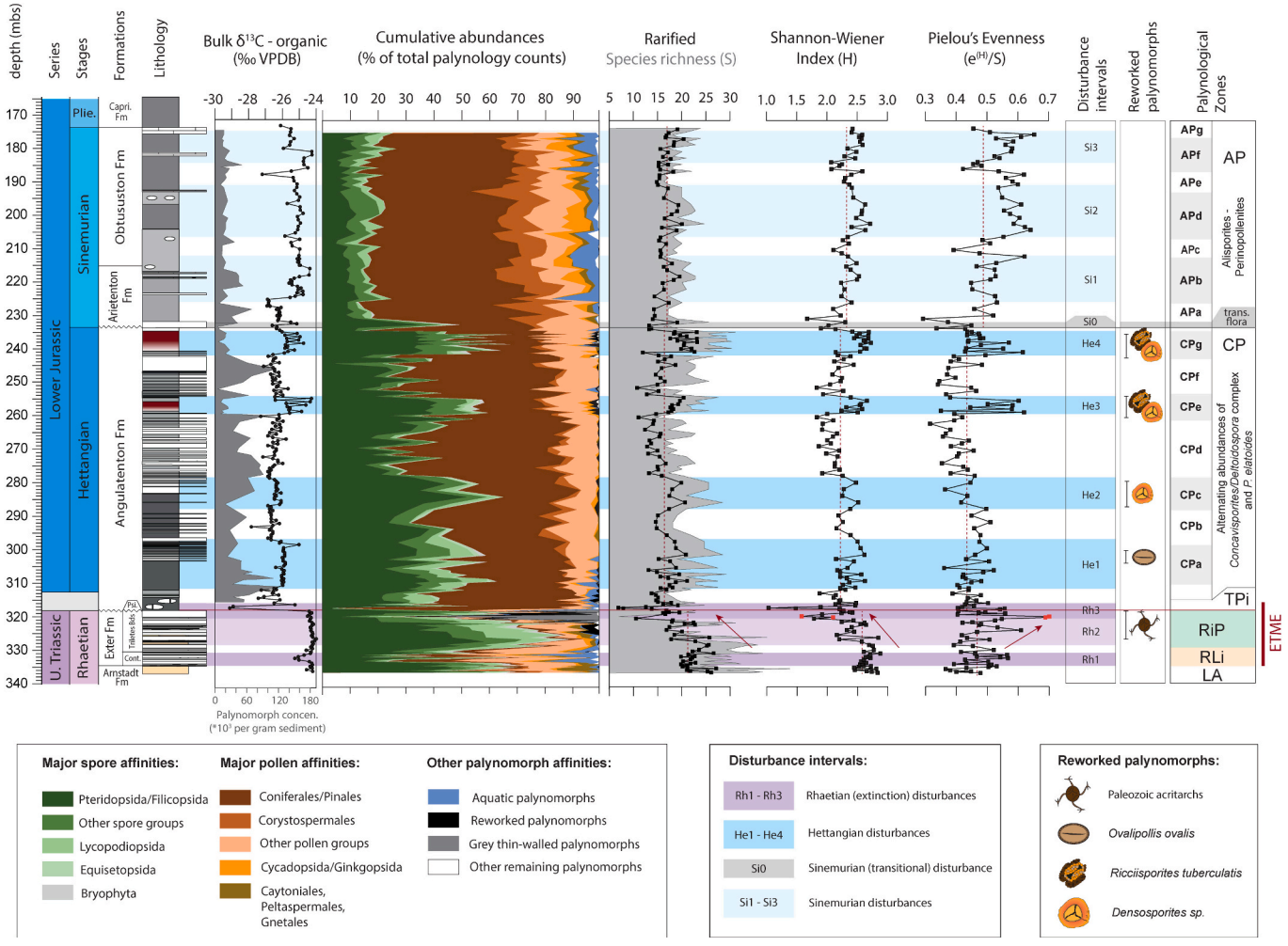

Fig. 5. Palynofloral diversity indices plotted against the variation of major botanical groups. Species richness, with non-rarified data given as grey-shaded area and rarified species richness as line with black squares for respective samples. Pielou's evenness and Shannon-Wiener Index (diversity) are given for terrestrial palynomorphs excluding aquatic, reworked and remaining palynomorphs. The median value for each index is indicated by a red dotted vertical line and separately calculated for each geological stage (Rhaetian, Hettangian and Sinemurian). Due to low rarefied species richness values, two samples are given by red squares. Horizontal coloured bars indicate position of disturbance intervals. Additional position of palynological zonation and reworked palynomorphs are indicated on the right-hand side of the graph. Absolute abundances of the total palynomorph assemblage were calculated using *Lycopodium* markers. (For interpretation of the references to colour in this figure legend, the reader is referred to the web version of this article.)

4.4. Palynofloral diversity

Diversity indices for palynofloral species are presented together with total palynological assemblages. These include richness, Shannon-Wiener index (SWI), and evenness (Fig. 5) and are based on their respective shifts in terrestrial palynological assemblage and depositional environments. This means we only included terrestrial palynomorphs and exclude reworked taxa. In addition, we compare the diversity indices with variation in absolute palynomorphs abundances.

The Rhaetian palynofloral composition shows several increases in evenness, both abrupt and short-lived (Rh1 and Rh3) and more gradual (Rh2). Increases in evenness are coupled to decreases in richness. The lowermost increase in evenness (Rh1) occurs within the Contorta Beds. The second abrupt shift (Rh3) is recorded within the uppermost Exter and lowermost Angulatenton formations and shows more substantial shifts in both evenness and richness. Palynofloral diversity across the Triletes Beds can largely be described by a general decrease in diversity towards the top of the Triletes Beds as observed in the richness and SWI curves (Fig. 5, Rh2). Positive correlation between all diversity indices and relative pollen abundance reveals the intricate relation between diversity and environment (Fig. S3, richness: $R^2 = 0.178$, SWI: $R^2 = 0.357$, evenness: $R^2 = 0.387$). These trends are similarly reflected in the decreasing TOC values of the same interval, indicated by positive correlations (Fig. S3: richness: $R^2 = 0.332$, SWI: $R^2 = 0.263$). The exception being evenness, which show low significance in relation with TOC ($R^2 = 0.053$).

Diversity dynamics across the Hettangian show a notable decrease in median richness, SWI and evenness compared to the Rhaetian records (Fig. 5). In addition, the diversity indices depict an in-phase pattern and reflects the observed variation in relative spore abundances associated with palynological subzones (CPa,c,e and g). Four distinct increases in richness and SWI (He1–4) coincide with similar increases in evenness. The exception is the He2 interval which does show increases in richness and SWI, but lower values of evenness. Specifically, the upper Hettangian increases in richness, SWI and evenness (He3–4) are most pronounced. The general pattern for the Hettangian palynofloral diversity indicates that cyclic increases in diversity are tightly coupled to increases in spore abundance, low absolute palynomorph abundances and positive carbon isotope excursions (Fig. 5). Positive correlations indicate spore-producing taxa is responsible to the increase in diversity (Fig. S3: richness: $R^2 = 0.537$, SWI: $R^2 = 0.559$, evenness; $R^2 = 0.269$). Therefore, we can infer that increases in diversity are driven by the expansion of pioneering fern taxa. TOC values show negative correlations across all three diversity indices (Fig. S3: richness: $R^2 = 0.154$, SWI: $R^2 = 0.189$, evenness: $R^2 = 0.164$).

The diversity indices within the Sinemurian records show a slight increase in median diversity (richness and SWI) and a more substantial increase in the median evenness compared to the Hettangian records. Simultaneous increases in richness, SWI and evenness can be recognized (Si1–3) which roughly coincide with palynological subzones (APb, d and f). This suggest that the increase in diversity is mainly linked to the increased abundance in wind-dispersed bisaccate pollen and several spore taxa. Positive correlations between the diversity indices and relative spore abundances (Fig. S3: richness: $R^2 = 0.221$, SWI: $R^2 = 0.310$, evenness: $R^2 = 0.232$) suggest that the spore taxa are largely responsible for the increases in diversity. TOC values reveal overall negative relationships with diversity indices that are of similar magnitudes as observed for the Hettangian palynoflora (Fig. S3: richness: $R^2 = 0.155$, SWI: $R^2 = 0.231$, evenness: $R^2 = 0.151$).

4.5. Time series analysis

We performed spectral analyses on the $\delta^{13}C_{org}$, magnetic susceptibility and spore/pollen (S/P) ratio records to assess the apparent periodic nature of the Hettangian strata of Schandelah-1 and phase-relations between vegetation and climate variability. Since there are several sedimentary facies shifts within the Schandelah-1 core, we isolated the Angulatenton Fm for spectral analysis. This formation is characterized with unconformity surfaces at the base and top. The duration of the Rhaetian deposits is largely based on the two negative CIEs that are closely tied to magmatic intrusions which might overprint any astronomical signal. The spectral analysis was performed in the depth domain and interpreted based on the relative ratios of the dominant cycles which are used to gain estimations of the duration of the Hettangian within the Schandelah-1 core.

The resulting power spectra reveal a dominant peak at 26.5 m/cycle (frequency = 0.045 cycles/m, robust AR(1) > 99%) on the bulk $\delta^{13}C_{org}$, magnetic susceptibility and S/P ratio series (Fig. 6B-D). Based on the estimated duration of the Hettangian which ranges from 1.7 to 2.3 Myr (Ruhl et al., 2010a; Hüsing et al., 2014; Xu et al., 2017; Storm et al., 2020) and the presence of 4 cycles, we hypothesize this cycle reflects the long-eccentricity (405-kyr) cycle, which is stable throughout the Mesozoic Era (Laskar et al., 2011). Other significant peaks are recorded at frequencies of 7.5 m, 2.7 m and 1.5 m, approximating ratios 20:5:2:1. We attribute these to short-eccentricity (96–135 kyr), obliquity (30–40 kyr) and precession cycle (18–25 kyr), respectively (Fig. 6B-D), also considering that the periodicities of precession and obliquity were shorter than in the present-day, namely ~20 kyr and ~35 kyr, respectively, due to long-term variation in the Earth-Moon system (Berger et al., 1989; House and Gale, 1995; Laskar, 2020). Additional dominant periods are observed for periods 63–69 kyr and 46 kyr. The origin of these frequencies remains unclear, but harmonic artifacts and/or interference patterns could be responsible.

Gaussian band-pass filters of the dominant 26.5 m/cycle (405 kyr) shows a good fit with all the analysed series (Fig. 6A). A near constant amplitude is noted for the carbon isotope record, while the amplitude seems to increase towards the top of the Hettangian for the MS filters with the highest amplitude correlating to the red clay intervals of the Angulatenton Fm. These show a similar increase in amplitude towards the top of the Hettangian. Furthermore, the amplitude modulation nature of the precession cycle by eccentricity seems to be most pronounced in the upper part of the Hettangian. Notable is the coinciding pattern of spore-dominated intervals with periods of high long-eccentricity cycles. Estimated duration of the Schandelah-1 Hettangian is 1.345 million years, which is lower than most estimations (Ruhl et al., 2010a; Hüsing et al., 2014; Xu et al., 2017; Storm et al., 2020). This is likely due to the unconformities recognized at the base and top of the Angulatenton Fm.

5. Discussion

5.1. Vegetation dynamics across the Late Triassic/Early Jurassic

The Late Triassic to Early Jurassic world was characterized by five distinct biomes dominated by upper canopy conifer trees (Willis and McElwain, 2014). These biomes include cool/warm temperate for higher latitudes, narrow bands of winter-wet biomes resembling Mediterranean regions and tropical summer-wet biomes in the lower latitudes. The latter were flanked by sub-tropical deserts to the north and south (Rees et al., 2000). Northward migration as a result of volcanic-triggered increases in greenhouse gasses and changing climatic conditions may have led to changes in distinct plant biomes across the European continent (Kent and Olsen, 2000; Rees et al., 2000; Sellwood and Valdes, 2006), although it is unclear how this major re-organisation of the global vegetation was facilitated.

Our palynological record from Schandelah-1 shows that the progression from the Rhaetian to the Sinemurian was marked by three distinct shifts in vegetation (Fig. 4). The recorded changes in vegetation composition appear to coincide with relative sea-level changes as inferred from changes in abundance of marine organic-walled microfossils (dinoflagellate cysts, acritarchs, foraminifera linings, prasinophytes). Algal palynomorphs and other aquatics show rapid and short-lived influxes during the Rhaetian, are generally absent during the

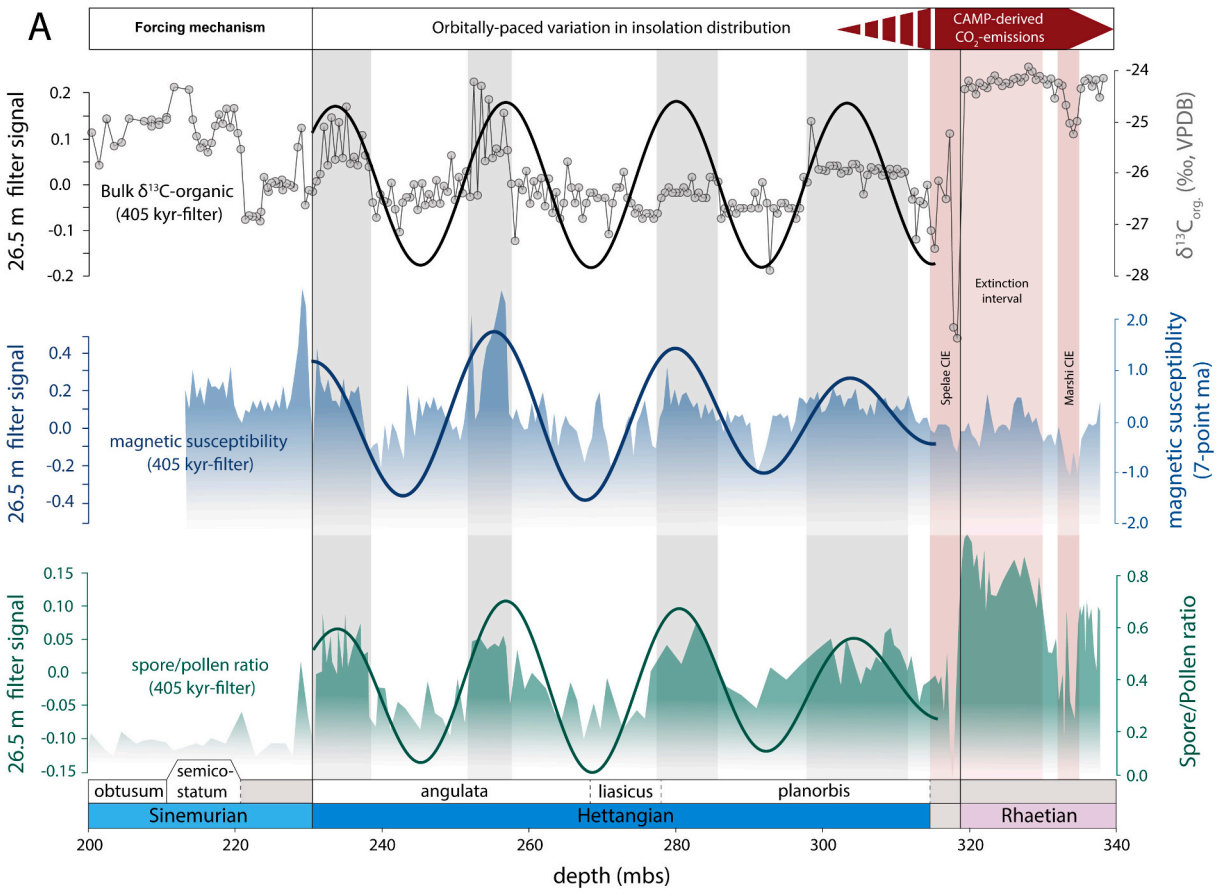

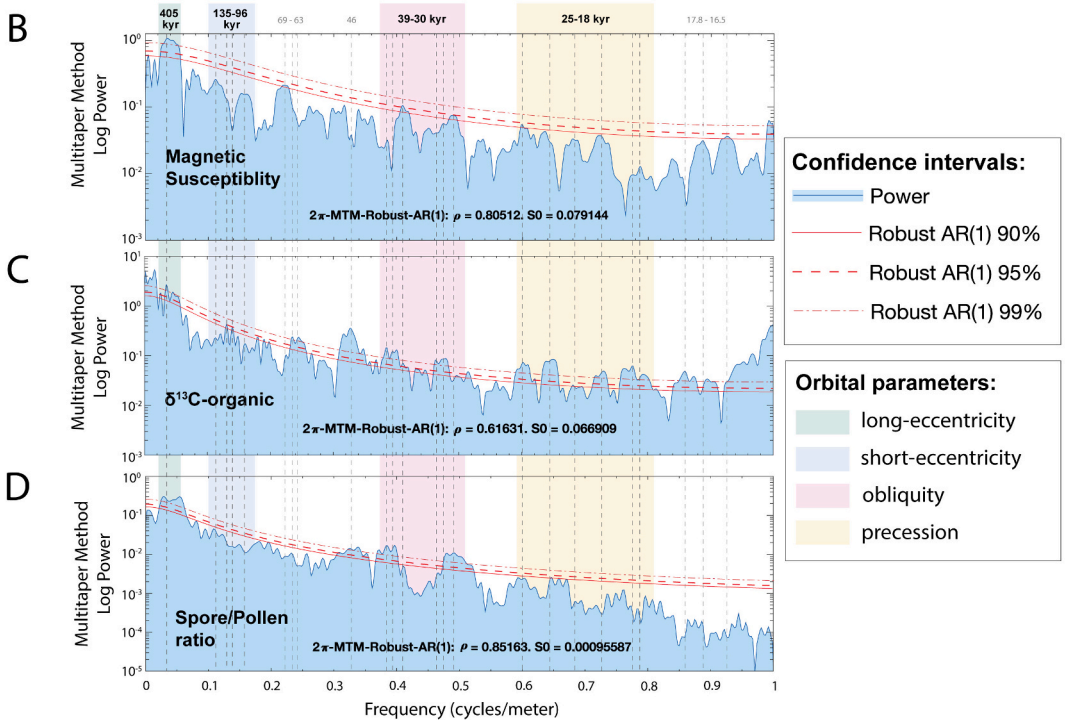

Fig. 6. Time series analysis of Schandelah-1 $\delta^{13}C_{org}$ and magnetic susceptibility records. **A.** Bandpass filters frequencies of the dominant spectral peaks. **B-C.** Multitaper method (MTM) power spectrum of magnetic susceptibility and $\delta^{13}C_{org}$ records. Dominant spectral peaks corresponding to 405 kyr long-eccentricity (green), ~135–96 kyr short-eccentricity (blue), ~39–30 kyr obliquity (pink) and ~ 25–18 kyr precession (yellow) are marked in figure. (For interpretation of the references to colour in this figure legend, the reader is referred to the web version of this article.)

Hettangian, and show a constant (although low) presence during the Sinemurian. Sea-level variations constitute a first order control on the preservation of organic matter (the Neves effect; Chaloner, 1958). However, the overall low abundances of aquatic (algal) taxa indicate a near-shore environment with only a minor influence of the Neves effect. Hence, assemblage changes and taxonomic losses of terrestrial palynomorphs reflect true changes in floral composition.

Severe taxonomic losses and mass rarity events proceeded in two distinct phases across the ETME, which are closely associated with two major negative CIEs (Gravendyck et al., 2020; Wignall and Atkinson, 2020; Lindström, 2021). In the Stenlille core in Denmark (Lindström, 2021) an initial decline in several pollen taxa, mostly belonging to upper canopy conifers, occurs directly after the Marshi CIE. This was followed by a proliferation of ground ferns and fern allies. The second episode of mass rarity coincides with the Spelae CIE and is mostly characterized by the disappearance of several taxa and a decline in the pioneering and disaster taxa that occupied the niches vacated by the initial disturbance. Similar results were reported for the Bonenberg section (Fig. 1) using diversity indices (Gravendyck et al., 2020). Generally, the interval between the two episodes of increased extinction is represented by increased abundance of *Polypodiisporites polymicroforatus* and has been taken as a marker for the "crisis interval" of the ETME (van de Schootbrugge et al., 2009; Lindström et al., 2012; Lindström, 2016). This "fern spike" interval can be traced across Europe and is recorded in St. Audrie's Bay (UK, Bonis et al., 2009), Stenlille (Denmark, Lindström et al., 2017), Mingholsheim (Germany, van de Schootbrugge et al., 2009), Kuhjoch (Austria, Bonis et al., 2010) and the Schandelah-1 core (this study).

These shifts in the vegetation are also expressed in various diversity indices (richness, SWI and evenness) that are commonly used in paleoecological studies to assess disturbance (Svensson et al., 2012). The relationship between biodiversity and ecosystem disturbance has classically been described by the Intermediate Disturbance Hypothesis (IDH). This hypothesis posits that stable and undisturbed ecosystems are represented by relatively few species. While increased diversity reflects ecosystem restructuring by successional stages of pioneering species in a stressed ecological community (Grim, 1973; Osman, 1977; Gravendyck et al., 2020). Intermediate disturbance interrupts the natural competitive process, prohibiting communities from maturing and reaching equilibrium. Simultaneous increases in richness and evenness reflects this interruption (Gravendyck et al., 2020; Lindström, 2021). Evenness in particular has been proposed to serve as an indicator for disturbance in the palynological record (Svensson et al., 2012; Gravendyck et al., 2020; Lindström, 2021). According to the IDH, increased evenness indicates continued and intensified disturbance. When combined with increased palynofloral richness, this reflects a successional stage (i.e., intermediate disturbance). On the other hand, increased evenness coupled with decreasing richness should be interpreted as disturbance beyond the intermediate level (i.e., extreme disturbance). Studies from ETME sections at Bonenberg (Gravendyck et al., 2020) and Stenlille (Lindström, 2021) have demonstrated that episodes of increased terrestrial extinction are also expressed through increased disturbance using diversity indices.

In the Rhaetian record of Schandelah-1, the first interval of disturbance is closely tied to the Marshi CIE (Fig. 5, Rh1) and is associated with a relative sea-level rise as noted by an influx of aquatic palynomorphs (Smith and McGowan, 2005; Peters and Foote, 2016; Lindström, 2021). It is not uncommon for coastal communities to be strongly influenced by variations in sea-level, which can cause salt stress (Seemann and Critchley, 1985; Pezeshki et al., 1990; Allen et al., 1996). This would explain the overall higher abundance of conifer pollen that rapidly diminish following the Marshi CIE. The overlying Triletes Beds show a gradual decline in taxonomic richness and a rapid increase in ground/tree ferns and clubmosses, suggesting a heavily disturbed ecosystem (Fig. 5, Rh2). This is further evident from a strong decline in nearly all pollen-producing groups, including the extinction of the Peltaspermalean seed ferns. However, the enigmatic gymnosperm that produced *Ricciisporites tuberculatus* shows increased abundances during this time and may have been the sole occupier of canopy and/or shrubby vegetation with minor influence of conifers (mainly *Classopollis* sp.). The resulting open landscape was largely colonized by shrubby and herbaceous vegetation dominated by ferns, horsetails, and seed ferns with a ground-layer of bryophyte mosses and clubmosses.

The second disturbance interval occurs at the transition from the Triletes Beds into the lowermost Angulatenton Fm (Fig. 5, Rh3). This second phase of environmental disturbance appears much more severe. High evenness values combined with a sharp decrease in richness and SWI indicates an extremely disturbed interval that is directly linked to the volcanic activity as evidenced by the negative carbon isotope excursion. It is important to note the presence of reworked Paleozoic palynomorphs and the extremely low TOC values (<0.2%) indicating a severe impact on paleo-productivity as soils were likely devastated by extreme weathering and erosion (van de Schootbrugge et al., 2020).

In contrast, the lowest value for richness occurs directly after the T-J boundary, synchronously with the Spelae CIE and an increase in TOC values. At this point we observe a clear shift to a vegetation with an Early Jurassic character. High TOC values within the lowermost Hettangian (Angulatenton Fm) can be attributed to increased marine primary production as reflected in high HI values. This level marks the onset of widespread anoxia across the European Epicontinental Seaway (Richoz et al., 2012), a likely contributing factor to the slow recovery in the marine realm (Wignall and Bond, 2008). Furthermore, the onset of the Spelae CIE (318.6–318.2 mbs) marks the disappearance of several important Rhaetian palynofloral taxa that include *R. tuberculatus*, *O. ovalis*, *L. rhaeticus*, *L. lundbladiae* and *Z. laevigatus* (Fig. 3). The disaster taxa of *P. polymicroforatus* which was dominant during the Triletes Beds similarly marks its last common occurrence at this horizon as well, indicating a substantial shift in vegetation.

The transition to the Early Jurassic is marked by an abrupt return of a conifer-dominated biome. Most notably, high abundances of conifers (*Classopollis*, *Pinuspollenites minimus* and *Perinopollenites elatoides*) provide evidence for a resurgence of closed-canopy forests (Fig. 4). Overall, this suggests drier conditions compared to the fern-dominated Triletes Beds. The early Hettangian is marked by another fern spike (CPa subzone), with a composition that is reminiscent of the late Rhaetian assemblage. However, disaster taxa such as *P. polymicroforatus* are not present in high numbers. The remainder of the Hettangian (CP zones b – g) is characterized by two distinct biomes that alternate in cyclic fashion between fern-dominated and conifer-dominated assemblages. Taken at face value, this would suggest alternating humid and dry periods. In addition, migration due to north-south oscillation of climate gradients (Kent and Olsen, 2000; Rees et al., 2000; Sellwood and Valdes, 2006) could also have led to changes in biome composition. Migration towards refugia allows entire plant biomes to cope and/or avoid climate perturbations as seen during the Quaternary glacial/interglacial cycles in southern Europe (Bennett et al., 1991) and even the Amazon (Bush, 1994). A major restructuring of vegetation during the Early Jurassic could have been driven by diversification and speciation in refugia.

The transition to the Sinemurian is characterized by a rapid shift towards a conifer-dominated vegetation with the expansion of several pollen-producing plant groups (Fig. 4, AP zone) and a general reduction in spore-producing plants. The lowermost Sinemurian (Arietes Sandstone, 233.3–230.2 mbs) is marked by the disappearance of several species. However, species richness indicates a brief increase followed by a rapid decrease (Fig. 5), which is paired with a substantial decrease in evenness. This boundary represents, therefore, another vegetation restructuring event for the northern German Basin. Most notably, we observe a significant change in the undergrowth, which is rich in seed ferns (Corystospermales and Caytoniales) and cycads/ginkgos (Fig. 4). Ferns strongly decrease in abundance, while fern allies, such as bryophytes are almost completely lacking. The dominance of bisaccate pollen indicates an increase in wind-pollinated trees, while the higher

numbers of aquatic palynomorphs indicate a shift towards more open marine conditions.

5.2. Mechanism driving ecosystem disturbance

5.2.1. Onset of the ETME

Mechanisms driving ecosystem disturbances can be divided into processes that restrict or alter biomass production, such as shifting climate conditions (temperature, precipitation), and processes that actively destroy biomass, such as wildfires and soil erosion. In addition, some plant groups may have profited from the vacant niches, as observed for the spread of pioneering fern taxa during the ETME crisis interval. Major conifer radiation during the Late Triassic is believed to have concurred with increasingly warm, seasonally wet/dry background conditions (Parrish, 1993). Major climate perturbations are commonly linked to changes in atmospheric greenhouse gasses. Elevated atmospheric pCO_2 would present a cascading effect on the continental interior of Pangea. Increasing continental temperature would increase evapotranspiration leading to decreased soil moisture, decreased convective precipitation and ultimately to widespread aridification (Peyser and Poulsen, 2008). In contrast, coastal regions developed seasonally flooded wetlands, which were fern-dominated and low in woody-taxa (McElwain et al., 1999; Bonis and Kürschner, 2012). The regional impact of changing global conditions should, therefore, be considered in order to develop a holistic model that explains the observed variation in vegetation.

Changes in the hydrological regime are evident within the palynofloral record of Schandelah-1. Most notably from variation in the dominance of moisture-preferring ferns/fern allies and dry-adapted gymnosperms. It is certainly true for the thermophilic and drought-adapted *Classopollis*-producing cheirolepid conifers (Abbink, 1998), but also the intermittent intervals that are dominated by ferns suggests that humidity may have limited conifer growth. Stratigraphically, an initial increase in microcharcoal abundance during the Rhaetian (326.5 mbs), which remains high in the Triletes Beds of Schandelah-1, suggests a stepwise progression of terrestrial disturbance (Fig. 4). An initial spike in wildfire activity and frequency strongly affected the conifer vegetation, which dominated the Contorta Beds and show a stepwise decrease in the Triletes Beds. Periods of enhanced precipitation caused a substantial decrease in soil stability and thus prevented the establishment of any stable biome. Ferns likely profited from the collapse of tree-forming vegetation as is evident by an increase in spore dominance in the Triletes Beds (Fig. 4). The crisis interval was dominated by several remaining disaster taxa such as *P. polymicroforatus* and *Aratrisporites minimus*, while other Late Triassic taxa only occurred sporadically and at low abundances. Wildfires still occurred in this spore-dominated interval, as indicated by microcharcoal abundance, but these were likely restricted to ground/surface and/or peat fires (Petersen and Lindstrom, 2012). Although elevated microcharcoal abundances could be explained through increased weathering and runoff, a decline in woody-taxa (mainly conifers) mirrors this trend and suggests that wildfire activity indeed influenced the vegetation composition.

High-amplitude climate variability would have triggered major swings in the hydrological regime. The low-latitude site of St. Audrie's Bay shows periodic changes in terrestrial palynomorph concentrations and spore abundances during the latest Rhaetian. This was mediated by changes in monsoonal activity forced by the 23-kyr precession cycle (Bonis et al., 2010). While elevated atmospheric CO_2 would result in widespread aridification within the inner Pangean continent (Peyser and Poulsen, 2008), coastal margins would be subjected to periods of enhanced precipitation (McElwain et al., 1999; Bonis and Kürschner, 2012). Increased humidity during late Rhaetian times has also been inferred based on elevated levels of kaolinite in boundary beds, suggestive of increased chemical weathering in the northern German Basin (van de Schootbrugge et al., 2009) and across Europe (Ahlberg et al., 2003; Pieńkowski et al., 2014; Zajzon et al., 2018). Moreover, shifts in the hydrological regime would also result in long intermittent periods of regional droughts increasing the likelihood of wildfires.

Enhanced levels of wildfire activity have been linked to major climatic perturbations in the geological past (Baker, 2022). T-J boundary sections in Greenland (Belcher et al., 2010; Williford et al., 2014) and Germany (Uhl and Montenari, 2011) show increased abundances of charcoal indicating increased wildfire activity. Also elevated levels of polycyclic aromatic hydrocarbons (PAHs) (Marynowski and Simoneit, 2009; Song et al., 2020) in boundary sediments in Poland and China have been taken as evidence for increased biomass burning. Additionally, increased atmospheric CO_2 levels may have favoured combustion-prone, narrow-leaved vegetation during the Late Triassic (Belcher et al., 2010), an effect that was further exacerbated by widespread droughts (Peyser and Poulsen, 2008). Petersen and Lindstrom (2012) suggested that the disappearance of Upper Rhaetian coal swamps in Denmark and their replacement by conifer forests was forced by wildfire activity.

Schandelah-1 provides evidence for major shifts in vegetation linked to carbon cycle perturbations. Carbon isotope records suggest a close link between organic matter sourcing and terrestrial vegetation composition. For the Late Triassic crisis and earliest Jurassic of Schandelah-1, TOC and Hydrogen Index seem to be closely tied to aquatic palynomorph abundance and also the abundance of most pollen-taxa (Fig. 2). Periods of high sea-level favoured the burial of mainly wind-dispersed conifers relative to coastal fern communities. This is most clear in the Contorta Beds which exhibits a simultaneous increase in TOC values and a negative (Marshi) CIE. This suggests a transgression partly influenced the vegetation composition and carbon isotope signal. However, the low TOC values of the overlying Triletes Beds indicate an active removal and/or prohibiting growth of terrestrial biomass. This interval shows little to no presence of aquatic palynomorphs and is characterized by relatively positive bulk $\delta^{13}C$ values.

The notable peak in Oxygen Index values at the top of the Triletes Beds indicates the input of woody and/or vascular plant remains, which are characterized by relatively high O/C values and low H/C values (Wignall, 1994; Killops and Killops, 2013). This correlates well with the reworked Paleozoic taxa and indicates a catastrophic failure of soils which culminates at the T-J boundary. An increase in grey thin-walled palynomorphs occurs simultaneous with the increase of reworked taxa, although the origin of these palynomorphs remains unclear, they are likely also reworked.

5.2.2. The main phase of the ETME

At the Triassic-Jurassic boundary the onset of the Spelae CIE exhibits a sharp ~5.8‰ shift. The nature of this CIE remains a topic of debate, also because the CIE varies in magnitude from site to site. However, based on a coinciding sharp increase in HI, the CIE can partly be explained by a shift in organic matter source, particular Type II kerogen of algal origin. The Spelae CIE in the St Audrie's Bay sections was interpreted to be driven by a transgression and increasing freshwater input causing the developments of microbial mats (Fox et al., 2022). This is substantiated by an increase of horsetail spores (*Calamospora tener*) suggesting increased riverine runoff. Similar observations have been made in the Stenlille sections (Denmark, Lindström, 2021). Although *C. tener* does occur during the lowermost Hettangian in Schandelah-1, this interval is most notably characterized by an acme of the dry-adapted *Classopollis*. This acme was also observed in the Eiberg Basin (Hochalpgraben, Bonis et al., 2009) and St. Audrie's Bay section (Bonis et al., 2010). In contrast, the Stenlille core shows an acme in mire-conifer pollen *Perinopollenites elatoides* at this level. The variability between sites could be the result of a strongly developed climate gradient, suggesting higher latitudes experienced wetter conditions, while the mid- and low-latitudes of the German and Eiberg Basins became overall drier (Lindström, 2021).

This seemingly variable trend in vegetation suggests that more than just CO_2 emissions were at play. Episodes of pulsed and/or explosive volcanism will release vast amounts of SO_2-emissions (Callegaro et al.,

2014; van de Schootbrugge and Wignall, 2016). SO_2-emissions act within a matter of weeks to months through atmospheric aerosols loading and cause global cooling, which can last for decades. On the same timescale of global cooling, additional effects of acid rain (H_2SO_4, HCl, HF) take hold. Additionally, volcanogenic SO_2-induced acid rain has the potential to alter soil conditions with the leaching and removal of essential cations (Ca, K and Mg) leading to lower soil pH. This would likely damage root systems, cause discolouration and loss of needles/leaves (Tomlinson, 2003). Acid rain would have a more devastating effect through sudden vegetation dieback, reduced photosynthetic capacity, increased cuticle damage, and a shift in competitive species composition. SO_2-fumigation is another proposed kill mechanism with a direct effect on epicuticular waxes such as lesions and distortions in the stomatal complex. Modern studies are proposing short inputs of highly concentrated SO_2 to be more impactful than long-term change (Haworth and McElwain, 2008). In contrast, long-term vegetation changes are facilitated through CO_2-induced global warming. CO_2 fertilisation leads to migration to high-latitude/coastal climate envelopes, sudden mass dieback through shifts in pathogen range (Wargo, 1996; Chakraborty et al., 2000; Yáñez-López, 2012) and decreased transpiration causing increased run-off and weathering rates (Wignall, 2001). The *Classopollis* acme in several European sites often transitions into an assemblage rich in spore-producing taxa. This likely reflects the long-term effects of CO_2 coming into effect.

The Spelae CIE is associated with both a transgression and extinctions in the marine realm (Richoz et al., 2012; van de Schootbrugge et al., 2013; Wignall and Atkinson, 2020). This transgression is expressed in the Schandelah-1 record by a lithology shift from sandstone to finely laminated shales, although this most likely didn't influenced the terrestrial climate and extinction (Hallam and Wignall, 1999). The marine impact is clearly reflected in multiple records across Europe and closely tied to volcanic CO_2 emissions. Before excess carbon could be removed via silicate weathering and carbon burial (Archer, 2005; Bachan and Payne, 2016), volcanic CO_2-injection caused immediate ocean acidification and global warming. These are considered as the main kill mechanisms for planktonic and benthic carbonate producers within 10 kyr or less (Bachan and Payne, 2016). In addition, evidence for photic zone euxinic conditions across sites in Europe and Canada has been noted at the T-J boundary (Wignall et al., 2007; Wignall and Bond, 2008; Richoz et al., 2012; Jaraula et al., 2013). The extent of euxinic conditions was likely limited to shallow seas (Richoz et al., 2012; Jaraula et al., 2013).

The semi-enclosed European Epicontinental Seaway was particularly sensitive to changes in the hydrological cycle and prone to water-column stratification, anoxia and prasinophyte algal blooms (Richoz et al., 2012). Mass occurrence of prasinophytes is often linked to black shale depositions (Riegel, 2008) and generally considered to indicate reduced salinity in surface waters. This was in many ways similar to the

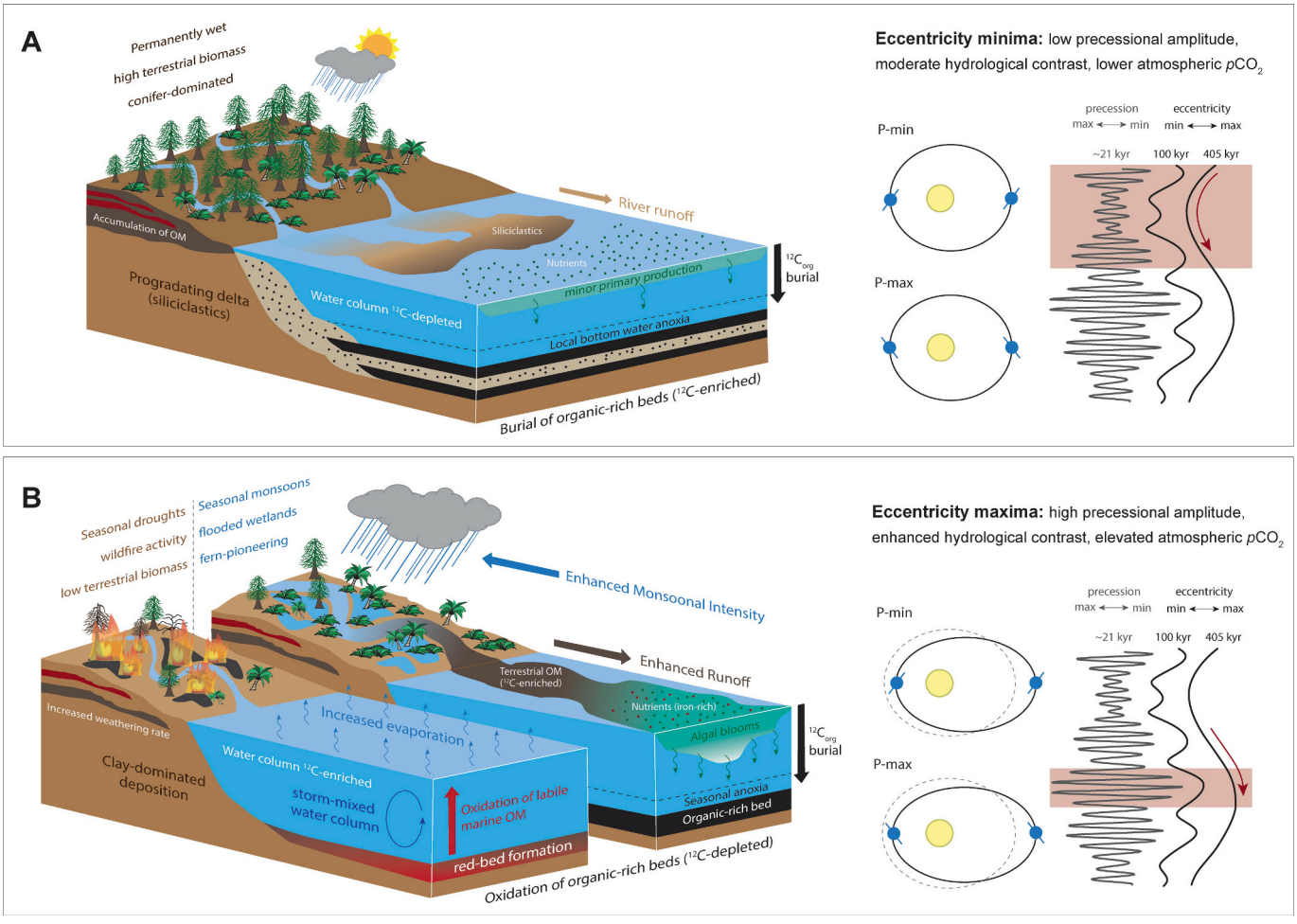

Fig. 7. Depositional model of paleoenvironmental changes in the northern German Basin, linked to eccentricity minima (A) and maxima (B) depicting variation in the hydrological cycle and its influence on terrestrial vegetation and carbon transport and burial. Phase relations with long and short eccentricity and precession are shown on the right. Red arrow indicates direction of astronomical progression. (For interpretation of the references to colour in this figure legend, the reader is referred to the web version of this article.)

volcanogenic-induced Ocean Anoxic Events (OAEs) during the Jurassic (e.g. Toarcian OAE) and Cretaceous (Hesselbo et al., 2000; Jenkyns, 2003; Mailliot et al., 2009). Black shale deposition is often associated with wetter climate conditions, as a response to volcanogenic CO_2-induced changes in the hydrological regime (Meyers et al., 2006). Salinity-driven stratification with a strong terrestrial influx (weathering) increased marine primary productivity, setting the stage of laminated sediment deposition (Mutterlose et al., 2009). Based on these proposed mechanisms, marine and terrestrial extinctions/disturbances should be closely intertwined. Indeed, independent examinations of marine faunal and algal extinctions (Wignall and Atkinson, 2020) and terrestrial mass rarity events (Lindström, 2021) show a synchronous decline in established fauna and flora during the crisis interval and culminates in synchronous disappearance of key species at the TJ Boundary.

5.3. Early Jurassic perturbations and orbital cycles

Early Jurassic climate forcing mechanisms differ from those during the Late Triassic. CAMP eruptions are estimated to have lasted for at least 600 thousand years, but no longer than 1 million years (Marzoli et al., 1999; Knight et al., 2004; Marzoli et al., 2004; Nomade et al., 2007). While some volcanic intrusives in the Eastern USA and Morocco clearly post-date the biotic crisis (Blackburn et al., 2013; Davies et al., 2017), their influence on Early Jurassic (Hettangian – Pliensbachian) climate is thought to have been limited. Instead, low-amplitude variations in bulk carbon isotope records (short-term shifts of 0.5–2 ‰) have been recorded for the Hettangian (Ruhl et al., 2010a; Hüsing et al., 2014; Xu et al., 2017) and Sinemurian (van de Schootbrugge et al., 2005; Jenkyns and Weedon, 2013; Riding et al., 2013; Porter et al., 2014; Xu et al., 2017; Hesselbo et al., 2020). These low-amplitude excursions are not driven by the injection of isotopically light carbon (^{12}C) derived from volcanic/thermogenic/biogenic sources (Hesselbo et al., 2002; McElwain et al., 2005). However, the exact mechanisms to explain these shifts remain enigmatic (Storm et al., 2020). But, given the cyclic nature of many of these records, orbital forcing played a key role.

The periodicities reported in many of the here presented records suggest a link between carbon cycle variation (bulk $\delta^{13}C_{org}$), detrital input (MS), and vegetation response (S/P ratio). Together these records point to changes in the regional hydrological regime (Fig. 7). Sites across the northern hemisphere would have experienced increased monsoonal activity during times of precession minima. Indeed, other Mesozoic periods show similar indications of annually dry climates with intervals of intense rainfall during eccentricity maxima (Martinez and Dera, 2015) when precessional amplitude was largest (Fig. 7B). Increased abundance of micro-charcoal indicating enhanced wildfire activity seems to follow the long-eccentricity cycle with an in-phase relation during eccentricity maxima (Fig. 7B). Similarly, during the Pliensbachian wildfire activity was prominent during periods of strong precession-forcing and maximum modulation of the 405-kyr eccentricity cycle (Hollaar et al., 2021). However, periods of high rainfall would alternate with long periods of drought during times of precession minima (Fig. 7B). This would limit the growth and establishment of conifer forests and promote the proliferation of fern and fern allies. Furthermore, periods of eccentricity maxima experienced prevailing dry conditions with a relatively higher sea-level stance. This is evident from periodic influxes of aquatic palynomorphs in the Schandelah-1 core.

Hettangian palynofloral assemblages therefore, responded to external forcing mechanisms linked to astronomical variation. The astronomical forcing is similarly observed in the alternations of laminated mudstone and fluvial/deltaic sandstone within the Schandelah-1 core. These laminated mudstone sequences are characterized by low TOC values and positive CIEs, and they are most clearly expressed in the upper half of the Angulatenton Fm. The presence of the fluvial/deltaic sandstone within laminated mudstone sequences indicate higher input of siliciclastic material with varying concentrations in TOC. These intervals are clearly reflected in the palynological record with sharp increases pteridopsid ferns (*Concavisporites* spp.) and fern allies, alternating with increases in the mire-conifer *Perinopollenites elatoides*. This indicates that the Hettangian palynofloral assemblage was overall comprised of vegetation that preferred wet/humid conditions. However, the continued presence of drought-adapted *Classopollis*-producing cheirolepid conifers does indicate drier periods as well (Abbink et al., 2001).

The Hettangian record of Schandelah-1 shows four periodic positive CIEs. Similar variation in HI and OI (Fig. 2) suggests that positive excursions in bulk $\delta^{13}C_{org}$ are partly indicative of shifts in organic matter sourcing. This indicates organics derived from low H/C sources are the main contributor to TOC. Alternative explanations include post-depositional oxidation, which are similarly characterized by high OI and low TOC values (Killops and Killops, 2013). This suggests that positive CIEs are the result of the degradation of labile (marine) organic matter, while preserving the refractory (terrestrial) organic matter. Overall, we infer that the main drivers of carbon isotopic shifts are characterized by the input/transport and burial/degradation of terrestrial organic matter.

Variation in insolation distribution through eccentricity-modulated precession was the main driver of climatic change during the Jurassic (Paillard, 2010; Martinez and Dera, 2015; Storm et al., 2020). During eccentricity minima the contrast in precessional amplitude was relatively lower, resulting in temperate conditions and low variability between precession minima and maxima (Fig. 7A). On the other hand, periods of eccentricity maxima would increase the contrast between precession minima and maxima, causing major swings in the hydrological regime (Landwehrs et al., 2022). Particular times of peak eccentricity maxima would result in major shifts in the northern hemisphere between cool/dry conditions (precession maxima) and warm/wet conditions (precession minima).

Precession and 100-kyr eccentricity cycles have been documented sections in the UK, modulating monsoonal intensity (terrestrial organic debris) and sea-level variation (Waterhouse, 1999). The proposed absence of major icesheets during the T-J interval, makes orbitally forced eustatic sea-level fluctuations unlikely (Frakes et al., 1992; Satterley, 1996; Hallam and Wignall, 1999). However, the aquifer-eustacy model suggest sea-level variation can be achieved through the storing and draining of water in continental aquifers and lakes during periods of humid and dry climates (Sames et al., 2016; Wendler and Wendler, 2016; Wendler et al., 2016; Noorbergen et al., 2018; Sames et al., 2020). It has been proposed that this system is forced via eccentricity-modulated climate change and can result in sea-level fluctuation of up to 30 m, periodically impacting coastal vegetation.

5.4. Recovery during the Sinemurian

The Sinemurian palynoflora of Schandelah-1 represents a stabilization in the vegetation, without indication of major environmental disturbances and higher diversity of pollen-bearing taxa. The lack of any major swings in palynofloral diversity and spore/pollen ratio suggests that vegetational recovery started during the early Sinemurian in Schandelah-1. The prevalence of the eccentricity minima system was most likely the cause for a return to pre-crisis conditions. This was achieved via a lowering of atmospheric CO_2 concentrations, inhibiting extreme climate conditions during eccentricity maxima. Recent estimates suggest ~2 million years of enhanced chemical weathering was required to drawdown excess atmospheric CO_2 after the initial carbon release event (CAMP activity) (Shen et al., 2022). This excess atmospheric CO_2 was removed through silicate weathering and long-term stored within organic-rich sediments (Archer, 2005). A widespread subsidence of the larger European Basin during the early Sinemurian, resulting in increased shallow marine accommodation space, would have aided the storage of carbon in both organic-rich beds and carbonate platforms. Furthermore, a long-term shift towards positive bulk $\delta^{13}C_{org}$ values from late Hettangian to mid-Sinemurian is evident in several UK

sections (Jenkyns and Weedon, 2013; Storm et al., 2020) and western North America (Porter et al., 2014). This possibly reflect long-term burial of carbon and reduced atmospheric CO_2 concentrations. The timing of vegetation recovery seems to have started in the Semicostatum ammonite zone, when bulk $\delta^{13}C_{org}$ values return to pre-ETME levels. Lower atmospheric CO_2 levels paved the way for a return to more stable conifer forests with a diverse understory comprising of seed ferns, cycads, ginkgos, ferns and fern allies.

6. Conclusions

The Schandelah-1 core provides a unique long-term archive of vegetation dynamics during and directly following the End-Triassic Mass-Extinction. A vegetation reconstruction based on high-resolution palynological analyses from Schandelah-1 is in line with previous work on other cores and outcrops for the ETME, but it allows us to provide a more detailed picture of the progression of vegetation recovery during the Early Jurassic.

Based on our high-resolution terrestrial palynological record, we find evidence for a stepwise vegetation turn-over during the ETME, with upper canopy conifers being transiently replaced by fern and fern allies, with the latter experiencing a major decline near the end of the biotic crisis. A dramatic decline in species richness combined with increasing evenness clearly indicates an extremely disturbed ecosystem. Geochemical records show that major changes in the palynological record are closely linked to negative carbon isotope excursions arising from pulsed CAMP-activity. However, based on various sites across Europe, it becomes clear that the effects of sea-level variation, most notably transgressions, also strongly influenced the decline of several pollen-taxa near the beginning of the biotic crisis. Evidence of wildfires, soil erosion and increased precipitation are identified as the main contributors to vegetation disturbance during the main crisis interval. Although the effects of other volcanic pollutants are difficult to gauge, evidence for short-lived shifts in climate, as inferred by successional stages in vegetation across the Triassic-Jurassic boundary, indicate the influence of SO_2-induced acid rain, which acts on short timescale. While other volcanic pollutants could also have played a role, the disappearance of many Triassic vegetation taxa are linked to a short-lived climate perturbation that acted as a final blow to already stressed ecosystem.

Terrestrial vegetation did not immediately recover from this major environmental upheaval, but instead shows evidence for major swings between stable conifer-dominated and disturbed fern-dominated intervals at regular pacing which is linked to variation in the long-eccentricity cycle (405 kyr). These swings are not just reflected in the palynology and diversity indices but are similarly observed in various geochemical records indicating a clear link between vegetation dynamics and climate change. These intervals of disturbances are reminiscent of the ETME successional stage and are similarly linked to wildfires, erosion and periodically intense rainfall. Here, similar proliferations of spore taxa are observed, combined with high diversity and evenness suggest an intermediately disturbed biome. Atmospheric CO_2 levels likely remained high after CAMP eruptions had ceased and likely plagued Hettangian biomes preventing the re-establishment of vegetation through astronomical-induced changes in the hydrological regime. Palynological data from Schandelah-1 indicates that the timing of vegetational recovery only occurred during the early Sinemurian synchronously with evidence for basin-wide subsidence/transgression. The reason for this recovery remains unclear, however, increased drawdown of atmospheric CO_2 through organic-rich and carbonate burial would have likely promoted more stable conditions.

Supplementary data to this article can be found online at https://doi.org/10.1016/j.gloplacha.2023.104211.

Declaration of Competing Interest

The authors declare the following financial interests/personal relationships which may be considered as potential competing interests: Bas van de Schootbrugge reports financial support was provided by Dutch Research Council.

Data availability

All data that is necessary to reach the conclusions in the study has been attached

Acknowledgements

We thank the crew, staff and sponsors of the Schandelah Scientific Drilling Project for their efforts in material recovery and providing us with the material and data studied in this report. This study was funded through the Dutch Research Council open program (NWO ALWOP.623) to whom we are grateful for providing us with the opportunity to conduct this research. We are grateful for the technical support at Utrecht University by Maxim Krasnoperov, Desmond Eefting, Arnold van Dijk, Giovanni Dammers and Natasja Welters.

References

Abbink, O.A., 1998. Palynological investigations in the Jurassic of the North Sea region. Lab. Palaeobot. Palynol. Utrecht 8, 141–154.
Abbink, O., Targarona, J., Brinkhuis, H., Visscher, H., 2001. Late Jurassic to earliest cretaceous palaeoclimatic evolution of the southern North Sea. Glob. Planet. Chang. 30 (3–4), 231–256.
Ahlberg, A., Olsson, I., Šimkevičius, P., 2003. Triassic–Jurassic weathering and clay mineral dispersal in basement areas and sedimentary basins of southern Sweden. Sediment. Geol. 161 (1–2), 15–29.
Allen, J.A., Pezeshki, S.R., Chambers, J.L., 1996. Interaction of flooding and salinity stress on baldcypress (Taxodium distichum). Tree Physiol. 16 (1–2), 307–313.
Alroy, J., 2008. Colloquium paper: dynamics of origination and extinction in the marine fossil record. Proc. Natl. Acad. Sci. U. S. A. 105 (Suppl. 1), 11536–11542.
Archer, D., 2005. Fate of fossil fuel CO2in geologic time. J. Geophys. Res. 110 (C9).
Askin, R.A., 1990. Campanian to Paleocene spore and pollen assemblages of Seymour Island, Antarctica. Rev. Palaeobot. Palynol. 65 (1–4), 105–113.
Bachan, A., Payne, J.L., 2016. Modelling the impact of pulsed CAMP volcanism onpCO2and δ13C across the Triassic–Jurassic transition. Geol. Mag. 153 (2), 252–270.
Baker, S.J., 2022. Fossil evidence that increased wildfire activity occurs in tandem with periods of global warming in Earth's past. Earth Sci. Rev. 224, 103871.
Balme, B.E., 1995. Fossil in situ spores and pollen grains: an annotated catalogue. Rev. Palaeobot. Palynol. 87 (2–4), 81–323.
Batten, D., Dutta, R., 1997. Ultrastructure of exine of gymnospermous pollen grains from Jurassic and basal cretaceous deposits in Northwest Europe and implications for botanical relationships. Rev. Palaeobot. Palynol. 99 (1), 25–54.
Beerling, D.J., Berner, R.A., 2002. Biogeochemical constraints on the Triassic-Jurassic boundary carbon cycle event. Glob. Biogeochem. Cycles 16 (3), 10-1-10-13.
Belcher, C.M., Mander, L., Rein, G., Jervis, F.X., Haworth, M., Hesselbo, S.P., Glasspool, I. J., McElwain, J.C., 2010. Increased fire activity at the Triassic/Jurassic boundary in Greenland due to climate-driven floral change. Nat. Geosci. 3 (6), 426–429.
Bennett, K., Tzedakis, P., Willis, K., 1991. Quaternary refugia of north European trees. J. Biogeogr. 103–115.
Benton, M.J., 1990. Scientific methodologies in collision: the history of the study of the extinction of the dinosaurs. Evol. Biol. 24 (37), 371–400.
Benton, M.J., 1995. Diversification and extinction in the history of life. Science 268 (5207), 52–58.
Berger, A., Loutre, M.F., Dehant, V., 1989. Astronomical frequencies for pre-Quaternary palaeoclimate studies. Terra Nova 1 (5), 474–479.
Blackburn, T.J., Olsen, P.E., Bowring, S.A., McLean, N.M., Kent, D.V., Puffer, J., McHone, G., Rasbury, E.T., Et-Touhami, M., 2013. Zircon U-Pb geochronology links the end-Triassic extinction with the Central Atlantic Magmatic Province. Science 340 (6135), 941–945.
Blakey, R.C., 2014. Paleogeography and paleotectonics of the western interior seaway, Jurassic-cretaceous of North America. Search Discov. 30392, 72.
Bond, D.P., Wignall, P.B., Keller, G., Kerr, A.C., 2014. Large igneous provinces and mass extinctions: an update. Volcanism, impacts, and mass extinctions: causes and effects, 505, pp. 29–55.
Bonis, N.R., Kürschner, W.M., 2012. Vegetation history, diversity patterns, and climate change across the Triassic/Jurassic boundary. Paleobiology 38 (2), 240–264.
Bonis, N.R., Kürschner, W.M., Krystyn, L., 2009. A detailed palynological study of the Triassic–Jurassic transition in key sections of the Eiberg Basin (Northern Calcareous Alps, Austria). Rev. Palaeobot. Palynol. 156 (3–4), 376–400.
Bonis, N.R., Ruhl, M., Kürschner, W.M., 2010. Climate change driven black shale deposition during the end-Triassic in the western Tethys. Palaeogeogr. Palaeoclimatol. Palaeoecol. 290 (1–4), 151–159.
Bush, M.B., 1994. Amazonian speciation: a necessarily complex model. J. Biogeogr. 5–17.

Callegaro, S., Baker, D.R., De Min, A., Marzoli, A., Geraki, K., Bertrand, H., Viti, C., Nestola, F., 2014. Microanalyses link sulfur from large igneous provinces and Mesozoic mass extinctions. Geology 42 (10), 895–898.
Caroff, M., Cotten, J., 2004. Geochemical evolution of a 10 m-thick intrusive body: the south Brenterc-h diabase dyke, Western Armorican Massif France. Can. J. Earth Sci. 41 (7), 775–784.
Cascales-Miñana, B.O.R.J.A., Cleal, C.J., 2012. Plant fossil record and survival analyses. Lethaia 45 (1), 71–82.
Chakraborty, S., Tiedemann, A.V., Teng, P.S., 2000. Climate change: potential impact on plant diseases. Environ. Pollut. 108 (3), 317–326.
Chaloner, W.G., 1958. The Carboniferous Upland Flora. Geol. Mag. 95 (3), 261–262.
Corso, J.D., Marzoli, A., Tateo, F., Jenkyns, H.C., Bertrand, H., Youbi, N., Mahmoudi, A., Font, E., Buratti, N., Cirilli, S., 2014. The dawn of CAMP volcanism and its bearing on the end-Triassic carbon cycle disruption. J. Geol. Soc. 171 (2), 153–164.
Davies, J., Marzoli, A., Bertrand, H., Youbi, N., Ernesto, M., Schaltegger, U., 2017. End-Triassic mass extinction started by intrusive CAMP activity. Nat. Commun. 8, 15596.
Deenen, M.H.L., Ruhl, M., Bonis, N.R., Krijgsman, W., Kuerschner, W.M., Reitsma, M., van Bergen, M.J., 2010. A new chronology for the end-Triassic mass extinction. Earth Planet. Sci. Lett. 291 (1–4), 113–125.
van Eldijk, T.J., Wappler, T., Strother, P.K., van der Weijst, C.M., Rajaei, H., Visscher, H., van de Schootbrugge, B., 2018. A Triassic-Jurassic window into the evolution of Lepidoptera. Sci. Adv. 4 (1), e1701568.
Elgorriaga, A., Escapa, I.H., Cúneo, N.R., 2019. RelictualLepidopteris(Peltaspermales) from the early Jurassic Cañadón Asfalto Formation, Patagonia, Argentina. Int. J. Plant Sci. 180 (6), 578–596.
Fox, C.P., Whiteside, J.H., Olsen, P.E., Cui, X., Summons, R.E., Idiz, E., Grice, K., 2022. Two-pronged kill mechanism at the end-Triassic mass extinction. Geology 50 (4), 448–453.
Frakes, L.A., Francis, J.E., Syktus, J.I., 1992. Climate modes of the Phanerozoic, pp. 286.
Golonka, J., Embry, A., Krobicki, M., 2018. Late triassic global plate tectonics. In: The Late Triassic World. Springer, Cham, pp. 27–57.
Gravendyck, J., Schobben, M., Bachelier, J.B., Kürschner, W.M., 2020. Macroecological patterns of the terrestrial vegetation history during the end-Triassic biotic crisis in the central European Basin: a palynological study of the Bonenburg section (NW-Germany) and its supra-regional implications. Glob. Planet. Chang. 194, 103286.
Grim, J.P., 1973. Competition and diversity in herbaceous vegetation (reply). Nature 244 (5414), 311.
Guignard, G., Wang, Y., Ni, Q., Tian, N., Jiang, Z., 2009. A dipteridaceous fern with in situ spores from the lower Jurassic in Hubei, China. Rev. Palaeobot. Palynol. 156 (1–2), 104–115.
Hallam, A., Wignall, P.B., 1999. Mass extinctions and sea-level changes. Earth Sci. Rev. 48 (4), 217–250.
Hammer, Ø., Harper, D.A., Ryan, P.D., 2001. PAST: Paleontological statistics software package for education and data analysis. Palaeontol. Electron. 4 (1), 9.
Harris, T.M., 1979. Equisetum filum sp. nov. from the Middle Jurassic of Yorkshire. Rev. Palaeobot. Palynol. 28 (2), 161–168.
Haworth, M., McElwain, J., 2008. Hot, dry, wet, cold or toxic? Revisiting the ecological significance of leaf and cuticular micromorphology. Palaeogeogr. Palaeoclimatol. Palaeoecol. 262 (1–2), 79–90.
Heimdal, T.H., Svensen, H.H., Ramezani, J., Iyer, K., Pereira, E., Rodrigues, R., Jones, M. T., Callegaro, S., 2018. Large-scale sill emplacement in Brazil as a trigger for the end-Triassic crisis. Sci. Rep. 8 (1), 1–12.
Hesselbo, S.P., Gröcke, D.R., Jenkyns, H.C., Bjerrum, C.J., Farrimond, P., Morgans Bell, H.S., Green, O.R., 2000. Massive dissociation of gas hydrate during a Jurassic oceanic anoxic event. Nature 406 (6794), 392–395.
Hesselbo, S.P., Robinson, S.A., Surlyk, F., Piasecki, S., 2002. Terrestrial and marine extinction at the Triassic-Jurassic boundary synchronized with major carbon-cycle perturbation: a link to initiation of massive volcanism? Geology 30 (3), 251–254.
Hesselbo, S.P., Hudson, A.J.L., Huggett, J.M., Leng, M.J., Riding, J.B., Ullmann, C.V., 2020. Palynological, geochemical, and mineralogical characteristics of the early Jurassic Liasidium Event in the Cleveland Basin, Yorkshire, UK. Newsl. Stratigr. 53 (2), 191–211.
von Hillebrandt, A., Krystyn, L., 2009. On the oldest Jurassic ammonites of Europe (Northern Calcareous Alps, Austria) and their global significance. N. Jb. Geol. Paläont. (Abh.) 253 (2–3), 163–195.
von Hillebrandt, A.V., Krystyn, L., Kuerschner, W.M., 2007. A candidate GSSP for the base of the Jurassic in the Northern Calcareous Alps (Kuhjoch section, Karwendel Mountains, Tyrol, Austria). Int. Subcomm. Jurassic Stratigr. Newslett. 34 (1), 2–20.
von Hillebrandt, A.V., Krystyn, L., Kürschner, W.M., Bonis, N.R., Ruhl, M., Richoz, S., Schobben, M.A.N., Urlichs, M., Bown, P.R., Kment, K., McRoberts, C.A., 2013. The global stratotype sections and point (GSSP) for the base of the Jurassic System at Kuhjoch (Karwendel Mountains, Northern Calcareous Alps, Tyrol, Austria). Episodes 36 (3), 162–198.
Hollaar, T.P., Baker, S.J., Hesselbo, S.P., Deconinck, J.-F., Mander, L., Ruhl, M., Belcher, C.M., 2021. Wildfire activity enhanced during phases of maximum orbital eccentricity and precessional forcing in the early Jurassic. Commun. Earth Environ. 2 (1), 1–12.
House, M.R., Gale, A.S., 1995. Orbital Forcing Timescales and Cyclostratigraphy, 85. Amer Assn of Petroleum Geologists.
Hüsing, S.K., Beniest, A., van der Boon, A., Abels, H.A., Deenen, M.H.L., Ruhl, M., Krijgsman, W., 2014. Astronomically-calibrated magnetostratigraphy of the lower Jurassic marine successions at St. Audrie's Bay and East Quantoxhead (Hettangian–Sinemurian; Somerset, UK). Palaeogeogr. Palaeoclimatol. Palaeoecol. 403, 43–56.
Jaraula, C.M.B., Grice, K., Twitchett, R.J., Böttcher, M.E., LeMetayer, P., Dastidar, A.G., Opazo, L.F., 2013. Elevated pCO2 leading to late Triassic extinction, persistent photic zone euxinia, and rising sea levels. Geology 41 (9), 955–958.
Jenkyns, H.C., 2003. Evidence for rapid climate change in the Mesozoic–Palaeogene greenhouse world. Philos. Trans. R. Soc. London, Ser. A 361 (1810), 1885–1916.
Jenkyns, H.C., Weedon, G.P., 2013. Chemostratigraphy (CaCO3, TOC, δ13Corg) of Sinemurian (lower Jurassic) black shales from the Wessex Basin, Dorset and palaeoenvironmental implications. Newsl. Stratigr. 46 (1), 1–21.
Kelber, K.-P., van Konijnenburg-van Cittert, J.H., 1998. Equisetites arenaceus from the Upper Triassic of Germany with evidence for reproductive strategies. Rev. Palaeobot. Palynol. 100 (1–2), 1–26.
Kent, D.V., Olsen, P.E., 2000. Magnetic polarity stratigraphy and paleolatitude of the Triassic-Jurassic Blomidon Formation in the Fundy basin (Canada): implications for early Mesozoic tropical climate gradients. Earth Planet. Sci. Lett. 179, 311–324.
Killops, V.J., Killops, S.D., 2013. Introduction to Organic Geochemistry. John Wiley & Sons.
Knight, K.B., Nomade, S., Renne, P.R., Marzoli, A., Bertrand, H., Youbi, N., 2004. The Central Atlantic Magmatic Province at the Triassic–Jurassic boundary: paleomagnetic and 40Ar/39Ar evidence from Morocco for brief, episodic volcanism. Earth Planet. Sci. Lett. 228 (1–2), 143–160.
van Konijnenburg-van Cittert, J.H., 1993. A review of the Matoniaceae based on in situ spores. Rev. Palaeobot. Palynol. 78 (3–4), 235–267.
van Konijnenburg-van Cittert, J., 2000. Pollen and Spores: Morphology and Biology. Royal Botanic Gardens Kew.
van Konijnenburg-Van Cittert, J., van der Burgh, J., 1989. The flora from the Kimmeridgian (Upper Jurassic) of Culgower, Sutherland, Scotland. Rev. Palaeobot. Palynol. 61 (1–2), 1–51.
van Konijnenburg-van Cittert, J.H.A., Pott, C., Schmeißner, S., Dütsch, G., Kustatscher, E., 2020. Ferns and fern allies in the Rhaetian flora of Wüstenwelsberg, Bavaria, Germany. Rev. Palaeobot. Palynol. 273, 104147.
van Konijnenburg-van Cittert, J.H.A., Pott, C., Schmeißner, S., Dütsch, G., Kustatscher, E., 2021. The Rhaetian flora of Wüstenwelsberg, Bavaria, Germany: Description of selected gymnosperms (Ginkgoales, Cycadales, Coniferales) together with an ecological assessment of the locally prevailing vegetation. Rev. Palaeobot. Palynol. 288, 104398.
van Konijnenburg-van Cittert, J.H., Schmeißner, S., Dütsch, G., Kustatscher, E., Pott, C., 2022. Plant macrofossils from the Rhaetian of Einberg near Coburg (Bavaria, Germany). Part 2. Cycadophyta and Ginkgophyta. Neues Jahrbuch für Geologie und Paläontologie-Abhandlungen, pp. 109–130.
Kuerschner, W.M., Bonis, N.R., Krystyn, L., 2007. Carbon-isotope stratigraphy and palynostratigraphy of the Triassic–Jurassic transition in the Tiefengraben section — Northern Calcareous Alps (Austria). Palaeogeogr. Palaeoclimatol. Palaeoecol. 244 (1–4), 257–280.
Lafargue, E., Marquis, F., Pillot, D., 1998. Rock-Eval 6 applications in hydrocarbon exploration, production, and soil contamination studies. Revue de l'institut français du pétrole 53 (4), 421–437.
Landwehrs, J., Feulner, G., Willeit, M., Petri, S., Sames, B., Wagreich, M., Whiteside, J.H., Olsen, P.E., 2022. Modes of Pangean lake level cyclicity driven by astronomical climate pacing modulated by continental position and pCO[Formula: see text]. Proc. Natl. Acad. Sci. U. S. A. 119 (46), e2203818119.
Laskar, J., 2020. Astrochronology, Geologic Time Scale 2020. Elsevier, pp. 139–158.
Laskar, J., Fienga, A., Gastineau, M., Manche, H., 2011. La2010: a new orbital solution for the long-term motion of the Earth. Astron. Astrophys. 532, A89.
Leslie, A.B., 2008. Interpreting the function of saccate pollen in ancient conifers and other seed plants. Int. J. Plant Sci. 169 (8), 1038–1045.
Li, L., Wang, Y., Liu, Z., Zhou, N., Wang, Y., 2016. Late Triassic palaeoclimate and palaeoecosystem variations inferred by palynological record in the northeastern Sichuan Basin, China. Paläontol. Z. 90 (2), 327–348.
Li, M., Hinnov, L., Kump, L., 2019. Acycle: Time-series analysis software for paleoclimate research and education. Comput. Geosci. 127, 12–22.
Li, L., Wang, Y., Kürschner, W.M., Ruhl, M., Vajda, V., 2020. Palaeovegetation and palaeoclimate changes across the Triassic–Jurassic transition in the Sichuan Basin, China. Palaeogeogr. Palaeoclimatol. Palaeoecol. 556, 109891.
Lindström, S., 2016. Palynofloral patterns of terrestrial ecosystem change during the end-Triassic event – a review. Geol. Mag. 153 (2), 223–251.
Lindström, S., 2021. Two-phased mass rarity and extinction in land plants during the end-triassic climate crisis. Front. Earth Sci. 9 (9), 1079.
Lindström, S., van de Schootbrugge, B., Dybkjaer, K., Pedersen, G.K., Fiebig, J., Nielsen, L.H., Richoz, S., 2012. No causal link between terrestrial ecosystem change and methane release during the end-Triassic mass extinction. Geology 40 (6), 531–534.
Lindström, S., Pedersen, G.K., van de Schootbrugge, B., Hansen, K.H., Kuhlmann, N., Thein, J., Johansson, L., Petersen, H.I., Alwmark, C., Dybkjær, K., Weibel, R., Erlström, M., Nielsen, L.H., Oschmann, W., Tegner, C., 2015. Intense and widespread seismicity during the end-Triassic mass extinction due to emplacement of a large igneous province. Geology 43 (5), 387–390.
Lindström, S., van de Schootbrugge, B., Hansen, K.H., Pedersen, G.K., Alsen, P., Thibault, N., Dybkjær, K., Bjerrum, C.J., Nielsen, L.H., 2017. A new correlation of Triassic–Jurassic boundary successions in NW Europe, Nevada and Peru, and the Central Atlantic Magmatic Province: A time-line for the end-Triassic mass extinction. Palaeogeogr. Palaeoclimatol. Palaeoecol. 478, 80–102.
Lindström, S., Sanei, H., Van De Schootbrugge, B., Pedersen, G.K., Lesher, C.E., Tegner, C., Heunisch, C., Dybkjær, K., Outridge, P.M., 2019. Volcanic mercury and mutagenesis in land plants during the end-Triassic mass extinction. Science. Advances 5 (10), eaaw4018.

Lindström, S., Callegaro, S., Davies, J., Tegner, C., van de Schootbrugge, B., Pedersen, G. K., Youbi, N., Sanei, H., Marzoli, A., 2021. Tracing volcanic emissions from the Central Atlantic Magmatic Province in the sedimentary record. Earth Sci. Rev. 212.
Looy, C.V., Collinson, M.E., Cittert, J.H.V.K.-V., Visscher, H., Brain, A.P., 2005. The ultrastructure and botanical affinity of end-Permian spore tetrads. Int. J. Plant Sci. 166 (5), 875–887.
Lund, J.J., 1977. Rhaetic to lower Liassic palynology of the onshore South-Eastern North Sea Basin. Danmarks Geologiske Undersøgelse II. Række 109, 1–128.
Mailliot, S., Mattioli, E., Bartolini, A., Baudin, F., Pittet, B., Guex, J., 2009. Late Pliensbachian–Early Toarcian (Early Jurassic) environmental changes in an epicontinental basin of NW Europe (Causses area, central France): A micropaleontological and geochemical approach. Palaeogeogr. Palaeoclimatol. Palaeoecol. 273 (3–4), 346–364.
Mander, L., 2011. Taxonomic resolution of the Triassic–Jurassic sporomorph record in East Greenland. J. Micropalaeontol. 30 (2), 107–118.
Mander, L., Kurschner, W.M., McElwain, J.C., 2010. An explanation for conflicting records of Triassic-Jurassic plant diversity. Proc. Natl. Acad. Sci. U. S. A. 107 (35), 15351–15356.
Mann, M.E., Lees, J.M., 1996. Robust estimation of background noise and signal detection in climatic time series. Clim. Chang. 33 (3), 409–445.
Manspeizer, W., 1994. The breakup of Pangea and its impact on climate: consequences of Variscan±Alleghanide orogenic collapse. Geol. Soc. Am. Spec. Pap. 288, 169–185.
Martindale, R.C., Corsetti, F.A., James, N.P., Bottjer, D.J., 2015. Paleogeographic trends in late Triassic reef ecology from northeastern Panthalassa. Earth Sci. Rev. 142, 18–37.
Martinez, M., Dera, G., 2015. Orbital pacing of carbon fluxes by a approximately 9-my eccentricity cycle during the Mesozoic. Proc. Natl. Acad. Sci. U. S. A. 112 (41), 12604–12609.
Marynowski, L., Simoneit, B.R.T., 2009. Widespread Upper Triassic to Lower Jurassic Wildfire Records from Poland: evidence from charcoal and pyrolytic polycyclic aromatic hydrocarbons. Palaios 24 (12), 785–798.
Marzoli, A., Renne, P.R., Piccirillo, E.M., Ernesto, M., Bellieni, G., Min, A.D., 1999. Extensive 200-million-year-old continental flood basalts of the Central Atlantic Magmatic Province. Science 284 (5414), 616–618.
Marzoli, A., Bertrand, H., Knight, K.B., Cirilli, S., Buratti, N., Vérati, C., Nomade, S., Renne, P.R., Youbi, N., Martini, R., Allenbach, K., Neuwerth, R., Rapaille, C., Zaninetti, L., Bellieni, G., 2004. Synchrony of the Central Atlantic magmatic province and the Triassic-Jurassic boundary climatic and biotic crisis. Geology 32 (11), 973–976.
McElwain, J.C., Punyasena, S.W., 2007. Mass extinction events and the plant fossil record. Trends Ecol. Evol. 22 (10), 548–557.
McElwain, J.C., Beerling, D.J., Woodward, F.I., 1999. Fossil plants and global warming at the Triassic-Jurassic boundary. Science 285 (5432), 1386–1390.
McElwain, J.C., Wade-Murphy, J., Hesselbo, S.P., 2005. Changes in carbon dioxide during an oceanic anoxic event linked to intrusion into Gondwana coals. Nature 435 (7041), 479–482.
McElwain, J.C., Popa, M.E., Hesselbo, S.P., Haworth, M., Surlyk, F., 2007. Macroecological responses of terrestrial vegetation to climatic and atmospheric change across the Triassic/Jurassic boundary in East Greenland. Paleobiology 33 (4), 547–573.
McElwain, J.C., Wagner, P.J., Hesselbo, S.P., 2009. Fossil plant relative abundances indicate sudden loss of late Triassic biodiversity in East Greenland. Science 324 (5934), 1554–1556.
McGhee, G.R., Clapham, M.E., Sheehan, P.M., Bottjer, D.J., Droser, M.L., 2013. A new ecological-severity ranking of major Phanerozoic biodiversity crises. Palaeogeogr. Palaeoclimatol. Palaeoecol. 370, 260–270.
Meyers, P.A., Bernasconi, S.M., Forster, A., 2006. Origins and accumulation of organic matter in expanded Albian to Santonian black shale sequences on the Demerara Rise, South American margin. Org. Geochem. 37 (12), 1816–1830.
Mutterlose, J., Pauly, S., Steuber, T., 2009. Temperature controlled deposition of early cretaceous (Barremian–early Aptian) black shales in an epicontinental sea. Palaeogeogr. Palaeoclimatol. Palaeoecol. 273 (3–4), 330–345.
Nomade, S., Knight, K.B., Beutel, E., Renne, P.R., Verati, C., Feraud, G., Marzoli, A., Youbi, N., Bertrand, H., 2007. Chronology of the Central Atlantic Magmatic Province: implications for the Central Atlantic rifting processes and the Triassic–Jurassic biotic crisis. Palaeogeogr. Palaeoclimatol. Palaeoecol. 244 (1–4), 326–344.
Noorbergen, L.J., Abels, H.A., Hilgen, F.J., Robson, B.E., de Jong, E., Dekkers, M.J., Krijgsman, W., Smit, J., Collinson, M.E., Kuiper, K.F., Fielding, C., 2018. Conceptual models for short-eccentricity-scale climate control on peat formation in a lower Palaeocene fluvial system, North-Eastern Montana (USA). Sedimentology 65 (3), 775–808.
Osborn, J.M., Taylor, T.N., de Lima, M.R., 1993. The ultrastructure of fossil ephedroid pollen with gnetalean affinities from the lower cretaceous of Brazil. Rev. Palaeobot. Palynol. 77 (3–4), 171–184.
Osman, R.W., 1977. The establishment and development of a marine epifaunal community. Ecol. Monogr. 47 (1), 37–63.
Paillard, D., 2010. Climate and the orbital parameters of the Earth. Compt. Rendus Geosci. 342 (4–5), 273–285.
Parrish, J.T., 1993. Climate of the supercontinent Pangea. J. Geol. 101 (2), 215–233.
Pedersen, K.R., Lund, J.J., 1980. Palynology of the plant-bearing rhaetian to Hettangian Kap Stewart formation, scoresby sund, East Greenland. Rev. Palaeobot. Palynol. 31, 1–69.
Peng, J., Li, J., Li, W., Slater, S.M., Zhu, H., Vajda, V., 2018. The Triassic to early Jurassic palynological record of the Tarim Basin, China. Palaeobiodivers. Palaeoenviron. 98 (1), 7–28.
Peters, S.E., Foote, M., 2016. Biodiversity in the Phanerozoic: a reinterpretation. Paleobiology 27 (4), 583–601.
Petersen, H.I., Lindstrom, S., 2012. Synchronous wildfire activity rise and mire deforestation at the triassic-jurassic boundary. PLoS One 7 (10), e47236.
Peyser, C.E., Poulsen, C.J., 2008. Controls on Permo-Carboniferous precipitation over tropical Pangaea: a GCM sensitivity study. Palaeogeogr. Palaeoclimatol. Palaeoecol. 268 (3–4), 181–192.
Pezeshki, S.R., DeLaune, R.D., Patrick Jr., W.H., 1990. Flooding and saltwater intrusion: potential effects on survival and productivity of wetland forests along the US Gulf Coast. For. Ecol. Manag. 33, 287–301.
Pieńkowski, G., Niedźwiedzki, G., Brański, P., 2014. Climatic reversals related to the Central Atlantic magmatic province caused the end-Triassic biotic crisis—evidence from continental strata in Poland. Volcanism, Impacts, and Mass Extinctions: Causes and Effects. Geol. Soc. Am. Spec. Pap. 505, 263–286.
Porter, S.J., Smith, P.L., Caruthers, A.H., Hou, P., Gröcke, D.R., Selby, D., 2014. New high resolution geochemistry of lower Jurassic marine sections in western North America: a global positive carbon isotope excursion in the Sinemurian? Earth Planet. Sci. Lett. 397, 19–31.
Rees, P.M., Ziegler, A.M., Valdes, P.J., Huber, B.T., Macleod, K.G., Wing, S.L., 2000. Jurassic phytogeography and climates: new data and model comparisons. Warm climates in earth history 297–318.
Richoz, S., van de Schootbrugge, B., Pross, J., Püttmann, W., Quan, T.M., Lindström, S., Heunisch, C., Fiebig, J., Maquil, R., Schouten, S., Hauzenberger, C.A., Wignall, P.B., 2012. Hydrogen sulphide poisoning of shallow seas following the end-Triassic extinction. Nat. Geosci. 5 (9), 662–667.
Riding, J.B., Leng, M.J., Kender, S., Hesselbo, S.P., Feist-Burkhardt, S., 2013. Isotopic and palynological evidence for a new early Jurassic environmental perturbation. Palaeogeogr. Palaeoclimatol. Palaeoecol. 374, 16–27.
Riegel, W., 2008. The late Palaeozoic phytoplankton blackout — Artefact or evidence of global change? Rev. Palaeobot. Palynol. 148 (2–4), 73–90.
Rudra, A., Sanei, H., Nytoft, H.P., Petersen, H.I., Blok, C., Bodin, S., Bojesen-Koefoed, J. A., 2021. Organic matter characterization of the lower cretaceous tight reservoirs in the Danish North Sea. Int. J. Coal Geol. 238, 103714.
Ruhl, M., Kürschner, W., 2011. Multiple phases of carbon cycle disturbance from large igneous province formation at the Triassic-Jurassic transition. Geology 39 (5), 431–434.
Ruhl, M., Deenen, M.H.L., Abels, H.A., Bonis, N.R., Krijgsman, W., Kürschner, W.M., 2010a. Astronomical constraints on the duration of the early Jurassic Hettangian stage and recovery rates following the end-Triassic mass extinction (St Audrie's Bay/East Quantoxhead, UK). Earth Planet. Sci. Lett. 295 (1–2), 262–276.
Ruhl, M., Veld, H., Kürschner, W.M., 2010b. Sedimentary organic matter characterization of the Triassic–Jurassic boundary GSSP at Kuhjoch (Austria). Earth Planet. Sci. Lett. 292 (1–2), 17–26.
Sames, B., Wagreich, M., Wendler, J.E., Haq, B.U., Conrad, C.P., Melinte-Dobrinescu, M. C., Hu, X., Wendler, I., Wolfgring, E., Yilmaz, I.Ö., Zorina, S.O., 2016. Review: short-term sea-level changes in a greenhouse world — a view from the cretaceous. Palaeogeogr. Palaeoclimatol. Palaeoecol. 441, 393–411.
Sames, B., Wagreich, M., Conrad, C.P., Iqbal, S., 2020. Aquifer-eustasy as the main driver of short-term sea-level fluctuations during cretaceous hothouse climate phases. Geol. Soc. Lond., Spec. Publ. 498 (1), 9–38.
Satterley, A.K., 1996. The interpretation of cyclic successions of the Middle and Upper Triassic of the Northern and Southern Alps. Earth Sci. Rev. 40 (3–4), 181–207.
Schaller, M.F., Wright, J.D., Kent, D.V., 2011. Atmospheric p CO2 perturbations associated with the Central Atlantic Magmatic Province. Science 331 (6023), 1404–1409.
Schaller, M.F., Wright, J.D., Kent, D.V., Olsen, P.E., 2012. Rapid emplacement of the Central Atlantic Magmatic Province as a net sink for CO2. Earth Planet. Sci. Lett. 323-324, 27–39.
Schaltegger, U., Guex, J., Bartolini, A., Schoene, B., Ovtcharova, M., 2008. Precise U–Pb age constraints for end-Triassic mass extinction, its correlation to volcanism and Hettangian post-extinction recovery. Earth Planet. Sci. Lett. 267 (1–2), 266–275.
Schobben, M., Gravendyck, J., Mangels, F., Struck, U., Bussert, R., Kürschner, W.M., Korn, D., Sander, P.M., Aberhan, M., 2019. A comparative study of total organic carbon-δ13C signatures in the Triassic–Jurassic transitional beds of the Central European Basin and western Tethys shelf seas. Newsl. Stratigr. 52 (4), 461–486.
Schoene, B., Latkoczy, C., Schaltegger, U., Günther, D., 2010. A new method integrating high-precision U–Pb geochronology with zircon trace element analysis (U–Pb TIMS-TEA). Geochim. Cosmochim. Acta 74 (24), 7144–7159.
van de Schootbrugge, B.A.S., Wignall, P.B., 2016. A tale of two extinctions: converging end-Permian and end-Triassic scenarios. Geol. Mag. 153 (2), 332–354.
van de Schootbrugge, B., McArthur, J.M., Bailey, T.R., Rosenthal, Y., Wright, J.D., Miller, K.G., 2005. Toarcian oceanic anoxic event: an assessment of global causes using belemnite C isotope records. Paleoceanography 20 (3).
van de Schootbrugge, B., Quan, T.M., Lindström, S., Püttmann, W., Heunisch, C., Pross, J., Fiebig, J., Petschick, R., Röhling, H.G., Richoz, S., Rosenthal, Y., Falkowski, P.G., 2009. Floral changes across the Triassic/Jurassic boundary linked to flood basalt volcanism. Nat. Geosci. 2 (8), 589–594.
van de Schootbrugge, B., Bachan, A., Suan, G., Richoz, S., Payne, J.L., Jagt, J., 2013. Microbes, mud and methane: cause and consequence of recurrent early Jurassic anoxia following the end-Triassic mass extinction. Palaeontology 56 (4), 685–709.
van de Schootbrugge, B., Richoz, S., Pross, J., Luppold, F.W., Hunze, S., Wonik, T., Blau, J., Meister, C., van der Weijst, C.M.H., Suan, G., Fraguas, A., Fiebig, J., Herrle, J.O., Guex, J., Little, C.T.S., Wignall, P.B., Püttmann, W., Oschmann, W., 2019. The Schandelah Scientific Drilling Project: a 25-million year record of early Jurassic palaeo-environmental change from northern Germany. Newsl. Stratigr. 52 (3), 249–296.

van de Schootbrugge, B., van der Weijst, C.M.H., Hollaar, T.P., Vecoli, M., Strother, P.K., Kuhlmann, N., Thein, J., Visscher, H., van Konijnenburg-van Cittert, H., Schobben, M.A.N., Sluijs, A., Lindström, S., 2020. Catastrophic soil loss associated with end-Triassic deforestation. Earth Sci. Rev. 210, 103332.
Scott, A.C., 2010. Charcoal recognition, taphonomy and uses in palaeoenvironmental analysis. Palaeogeogr. Palaeoclimatol. Palaeoecol. 291 (1–2), 11–39.
Seemann, J.R., Critchley, C., 1985. Effects of salt stress on the growth, ion content, stomatal behaviour and photosynthetic capacity of a salt-sensitive species. *Phaseolus vulgaris* L. Planta 164 (2), 151–162.
Sellwood, B.W., Valdes, P.J., 2006. Mesozoic climates: General circulation models and the rock record. Sediment. Geol. 190 (1–4), 269–287.
Shannon, C.E., Weaver, W., 1949. The Mathematical Theory of Information, vol. 97(6). University of Illinois Press, Urbana, pp. 128–164.
Shen, J., Yin, R., Zhang, S., Algeo, T.J., Bottjer, D.J., Yu, J., Xu, G., Penman, D., Wang, Y., Li, L., Shi, X., Planavsky, N.J., Feng, Q., Xie, S., 2022. Intensified continental chemical weathering and carbon-cycle perturbations linked to volcanism during the Triassic-Jurassic transition. Nat. Commun. 13 (1), 299.
Smith, A.B., McGowan, A.J., 2005. Cyclicity in the fossil record mirrors rock outcrop area. Biol. Lett. 1 (4), 443–445.
Song, Y., Algeo, T.J., Wu, W., Luo, G., Li, L., Wang, Y., Xie, S., 2020. Distribution of pyrolytic PAHs across the Triassic-Jurassic boundary in the Sichuan Basin, southwestern China: evidence of wildfire outside the Central Atlantic Magmatic Province. Earth Sci. Rev. 201, 102970.
Steinthorsdottir, M., Jeram, A.J., McElwain, J.C., 2011. Extremely elevated CO2 concentrations at the Triassic/Jurassic boundary. Palaeogeogr. Palaeoclimatol. Palaeoecol. 308 (3–4), 418–432.
Storm, M.S., Hesselbo, S.P., Jenkyns, H.C., Ruhl, M., Ullmann, C.V., Xu, W., Leng, M.J., Riding, J.B., Gorbanenko, O., 2020. Orbital pacing and secular evolution of the early Jurassic carbon cycle. Proc. Natl. Acad. Sci. U. S. A. 117 (8), 3974–3982.
Svensson, J.R., Lindegarth, M., Jonsson, P.R., Pavia, H., 2012. Disturbance-diversity models: what do they really predict and how are they tested? Proc. Biol. Sci. 279 (1736), 2163–2170.
Tomlinson, G.H., 2003. Acidic deposition, nutrient leaching and forest growth. Biogeochemistry 65 (1), 51–81.
Traverse, A., 2007. Holocene palynology. In: Paleopalynology. Springer, pp. 463–495.
Uhl, D., Montenari, M., 2011. Charcoal as evidence of palaeo-wildfires in the late Triassic of SW Germany. Geol. J. 46 (1), 34–41.
Wargo, P.M., 1996. Consequences of environmental stress on oak: predisposition to pathogens. In Annales des sciences forestières 53 (2–3), 359–368.
Waterhouse, H.K., 1999. Orbital forcing of palynofacies in the Jurassic of France and the United Kingdom. Geology 27 (6), 511–514.
Wendler, J.E., Wendler, I., 2016. What drove sea-level fluctuations during the mid-cretaceous greenhouse climate? Palaeogeogr. Palaeoclimatol. Palaeoecol. 441, 412–419.
Wendler, J.E., Wendler, I., Vogt, C., Kuss, J., 2016. Link between cyclic eustatic sea-level change and continental weathering: evidence for aquifer-eustasy in the cretaceous. Palaeogeogr. Palaeoclimatol. Palaeoecol. 441, 430–437.
Whiteside, J.H., Olsen, P.E., Eglinton, T., Brookfield, M.E., Sambrotto, R.N., 2010. Compound-specific carbon isotopes from Earth's largest flood basalt eruptions directly linked to the end-Triassic mass extinction. Proc. Natl. Acad. Sci. U. S. A. 107 (15), 6721–6725.
Wignall, P.B., 1994. Mudstone Lithofacies in the Kimmeridge Clay Formation, Wessex Basin, Southern England: Implications for the Origin and Controls of the distribution of Mudstones: DISCUSSION. J. Sediment. Res. 64 (4).
Wignall, P.B., 2001. Large igneous provinces and mass extinctions. Earth Sci. Rev. 53 (1–2), 1–33.
Wignall, P.B., Atkinson, J.W., 2020. A two-phase end-Triassic mass extinction. Earth Sci. Rev. 208, 103282.
Wignall, P.B., Bond, D.P., 2008. The end-Triassic and early Jurassic mass extinction records in the British Isles. Proc. Geol. Assoc. 119 (1), 73–84.
Wignall, P.B., Zonneveld, J.P., Newton, R.J., Amor, K., Sephton, M.A., Hartley, S., 2007. The end Triassic mass extinction record of Williston Lake, British Columbia. Palaeogeogr. Palaeoclimatol. Palaeoecol. 253 (3–4), 385–406.
Williford, K.H., Grice, K., Holman, A., McElwain, J.C., 2014. An organic record of terrestrial ecosystem collapse and recovery at the Triassic–Jurassic boundary in East Greenland. Geochim. Cosmochim. Acta 127, 251–263.
Willis, K., McElwain, J., 2014. The Evolution of Plants. Oxford University Press.
Xu, C., Zhang, L., Shi, H., Brix, M.R., Huhma, H., Chen, L., Zhang, M., Zhou, Z., 2017. Tracing an early Jurassic magmatic arc from South to East China Seas. Tectonics 36 (3), 466–492.
Yáñez-López, R., 2012. The effect of climate change on plant diseases. Afr. J. Biotechnol. 11 (10), 2417–2428.
Zajzon, N., Kristály, F., Pálfy, J., Németh, T., 2018. Detailed clay mineralogy of the Triassic-Jurassic boundary section at Kendlbachgraben (Northern Calcareous Alps, Austria). Clay Miner. 47 (2), 177–189.